

This is the accepted version of the following article:

Mohammad Rahman, Kenneth Davey, and Shi-Zhang Qiao  
**Advent of 2D rhenium disulfide (ReS<sub>2</sub>): fundamentals to applications**  
Advanced Functional Materials, 2017; 27(10):1606129-1-1606129-21

© 2017 WILEY-VCH Verlag GmbH & Co. KGaA, Weinheim

Which has been published in final form at <http://dx.doi.org/10.1002/adfm.201606129>

This article may be used for non-commercial purposes in accordance with the Wiley Self- Archiving Policy <http://olabout.wiley.com/WileyCDA/Section/id-828039.html>

## PERMISSIONS

<http://www.wiley-vch.de/cta/physsci-en>

**2. Accepted Version.** Wiley-VCH licenses back the following rights to the Contributor in the version of the Contribution that has been peer-reviewed and accepted for publication, but not final (the "Accepted Version"):

a. The right to self-archive the Accepted Version on the Contributor's personal website, in the Contributor's company/institutional repository or archive, in Compliant SCNs, and in not for profit subject-based repositories such as PubMed Central, subject to an embargo period of 12 months following publication of the Final Published Version. There are separate arrangements with certain funding agencies governing reuse of the Accepted Version as set forth at the following website: [www.wiley.com/go/funderstatement](http://www.wiley.com/go/funderstatement). The Contributor may not update the Accepted Version or replace it with the Final Published Version. The Accepted Version posted

must contain a legend as follows: This is the accepted version of the following article: FULL CITE, which has been published in final form at [Link to final article]. This article may be used for non-commercial purposes in accordance with the Wiley Self-Archiving Policy [olabout.wiley.com/WileyCDA/Section/id-820227.html].

8 March 2018

<http://hdl.handle.net/2440/103880>

1 DOI: 10.1002/ ((please add manuscript number))

2  
3 **Article Type: (Feature Article)**

4  
5  
6  
7 **Advent of 2D Rhenium Disulfide (ReS<sub>2</sub>): Fundamentals to Applications**

8  
9  
10 *Mohammad Rahman, Kenneth Davey and Shi-Zhang Qiao\**

11  
12  
13  
14 M. Z. Rahman, Dr. K. Davey, Prof. S. Z. Qiao  
15 School of Chemical Engineering, The University of Adelaide, SA 5005, Australia  
16 E-mail: s.qiao@adelaide.edu.au  
17

18  
19  
20 **Abstract**

21  
22 Rhenium disulfide (ReS<sub>2</sub>) is a two dimensional (2D) group VII transition metal  
23 dichalcogenide (TMD). It is attributed with structural and vibrational anisotropy, layer  
24 independent electrical and optical properties, and metal-free magnetism properties. These  
25 properties are unusual compared with more widely used group VI-TMDs e.g. MoS<sub>2</sub>, MoSe<sub>2</sub>,  
26 WS<sub>2</sub> and WSe<sub>2</sub>. Consequently, it has attracted significant interest in recent years and is now  
27 being used for a variety of applications including solid state electronics, catalysis, and, energy  
28 harvesting and energy storage. **It is anticipated that ReS<sub>2</sub> has the potential to be equally used**  
29 **in parallel with isotropic TMDs from group VI for all known applications and beyond.**  
30  
31 Therefore, a review on ReS<sub>2</sub> is very timely. In this first review on ReS<sub>2</sub>, we critically analyze  
32 the available synthesis procedures and their pros-cons, atomic structure and lattice symmetry,  
33 crystal structure and growth mechanisms with an insight to the orientation and architecture of  
34 domain and grain boundaries, decoupling of structural and vibrational properties, anisotropic  
35 electrical, optical and magnetic properties impacted by crystal imperfections, doping and  
36 adatoms adsorptions, and the contemporary applications in different areas.  
37  
38  
39  
40  
41  
42  
43  
44  
45  
46  
47  
48  
49  
50  
51  
52  
53  
54  
55  
56

57 **Keywords:** *Rhenium disulfide, transition metal dichalcogenide, device fabrication, energy*  
58 *conversion, energy storage*  
59

## 1. Introduction

Two dimensional (2D) materials today are a priority choice for research and application in almost every area of science and engineering. Despite a near-century long debate on existence of 2D materials, the discovery of graphene in 2004 began a new paradigm of naturally existing 2D materials.<sup>[1, 2]</sup> However, graphene is a zero bandgap material and is not suitable for applications where a bandgap is required. Therefore research is being directed toward new 2D materials. As a result, an almost avalanche of research has resulted into flat materials beyond carbon species e.g. graphene culminated with a new genre of materials that have identical features of classic 2D materials, but with additional beneficial properties that graphene lacks.<sup>[3, 4, 5]</sup> Silicon (Si), tin (Sn), black phosphorous (BP), germanium (Ge), transition metal dichalcogenides (TMDs), and transition metal trichalcogenides (TMTCs)<sup>[6, 7, 8]</sup> are the main contributors to this new class of 2D materials in the post-graphene era. Analogous to graphene, single layers of Si, Sn, BP and Ge are also affixed with the suffix 'ene' to distinguish the monolayer from bulk materials. For example, silicene, stanene, phosphorene, germenene are monolayers of bulk Si, Sn, BP and Ge, respectively.<sup>[3, 9]</sup> Whilst there is some ongoing dispute about scalable synthesis and stability of performances of silicene, stanene, phosphorene, and germenene, monolayers of TMDs are relatively easy to exfoliate, affordable, accessible, and are highly reliable.<sup>[10-12]</sup> Therefore, TMDs are a priority in 2D flat materials over graphene.

Monolayer TMDs are 2D materials consisting of an atomic plane of transition metal (Mo, W, Ti, Nb, Re, V, Zr, Ta, Hf etc.) sandwiched between two chalcogen planes (S, Se, Te).<sup>[13, 14]</sup> A wide variety of TMDs therefore can be obtained with diverse and controlled electronic properties. A ball and stick diagram of typical TMD, and 2D transition metals (marked green) in the periodic table is presented in **Figure 1**. TMDs have been known since 1960, and in fact a group of 40 TMDs and their basic properties was reviewed in 1969.<sup>[15]</sup> Group VI materials,

1 such as Mo and W, are the most representative TMDs. Aside from the most popular TMDs of  
2  
3 group VI, rhenium disulfide (ReS<sub>2</sub>, an example of group VII TMDs) has recently attracted  
4  
5 significant interest for its wholly unusual properties in all aspects of structural, electro-optical  
6  
7 and chemical properties.<sup>[16, 17]</sup> Most notably, an indirect to direct transition is obvious for  
8  
9 group VI-TMDs when thinned down to monolayer from the bulk material.<sup>[18, 19]</sup> Whilst  
10  
11 different to other TMDs, ReS<sub>2</sub> has shown layer independent electrical, optical and vibrational  
12  
13 properties.<sup>[20]</sup> In addition, widely studied group VI-TMDs possess 1H, 2H, 3R or 1T  
14  
15 molecular structure while ReS<sub>2</sub> exhibits unique distorted 1T structure giving it to an in-plane  
16  
17 anisotropy in fundamental physical properties.<sup>[21]</sup> It is to be noted that there exists only a  
18  
19 small number of materials (i.e. BP, ReS<sub>2</sub>, ReSe<sub>2</sub>, TiS<sub>3</sub>, ZrS<sub>3</sub>) with in-plane structural  
20  
21 anisotropy.<sup>[7, 8, 22, 23]</sup> These benchmark properties make ReS<sub>2</sub> a unique material among the  
22  
23 TMDs.  
24  
25  
26  
27  
28

29 ReS<sub>2</sub> is comprised of three atomic layers, S-Re-S, where Re and S are joined by covalent  
30  
31 bonds. Like other flagship 2D materials, the adjacent layers in ReS<sub>2</sub> are also coupled by weak  
32  
33 van der Waals (vdW) forces to form bulk crystals. Its unit cell is derived from hexagonal  
34  
35 symmetry towards a distorted 1T structure, in which Re atoms group into parallelograms of  
36  
37 four Re atoms, thereby enabling prodigious possibilities to introduce built-in planar  
38  
39 anisotropy into composite heterostructures.<sup>[17, 24]</sup> The added advantages of ReS<sub>2</sub> are that it is a  
40  
41 flexible semiconductor that has additional possibilities to tune properties with doping and  
42  
43 coupling with other materials.<sup>[25-27]</sup> This implies overall that if a 2D ReS<sub>2</sub> is wanted as a  
44  
45 semiconductor with a given set of properties, it is sure to find one. Moreover, ReS<sub>2</sub> is  
46  
47 dichalcogenide, but shows anisotropy like trichalcogenides (i.e. TiS<sub>3</sub>, ZrS<sub>3</sub> etc.)  
48  
49  
50  
51  
52  
53

54 In-line with, as well as in-contrast with other 2D materials, ReS<sub>2</sub> is attributed with the  
55  
56 following gross features:<sup>[28, 29]</sup> (i) alike other 2D materials, 2D ReS<sub>2</sub> exhibits a wide range of  
57  
58 unique physicochemical properties. In contrast, whilst other 2D materials show dissimilar but  
59  
60  
61  
62  
63  
64  
65

1 unique physicochemical properties to that of 3D bulk counter part, both 2D and 3D ReS<sub>2</sub>  
2 show no different physicochemical properties, (ii) whilst the optical and optoelectronic  
3 properties of 2D layered semiconductors are reliant on the number of layers and the changes  
4 in symmetry as a consequence of quantum confinement effects in the out-of-plane direction,  
5 ReS<sub>2</sub> shows nearly layer-independent optoelectronic properties, (iii) due to a dimensionality  
6 confinement effect and modulation in band structure, a shift in optical absorption from infra-  
7 red (IR) to ultraviolet (UV) light is literally inevitable in other 2D materials except ReS<sub>2</sub>, (iv)  
8 like other 2D functional materials, it is also mechanically flexible, and interacts strongly with  
9 incident light which can lead to enhanced photon absorption and electron-hole pairs (EHPs)  
10 generation, and; (v) due to vdW interaction between the layers and no surface dangling bonds,  
11 it offers significant opportunities to design many functional heterostructures by integration  
12 with other materials without concern due to limitations with lattice matching.

13 **Because of these distinguishable properties, ReS<sub>2</sub> is an emerging material for applications**  
14 **in which other 2D materials are also currently being exploited.** It is now being used, for  
15 example, for fabrication of solid state devices, photo-electro catalytic energy conversion, and  
16 storage. In devices fabrication ReS<sub>2</sub> supplants graphene. This is because, despite the  
17 superlatives physicists have used to describe the attractiveness of graphene, it's lack of a  
18 bandgap makes it all but useless where a semiconductor is needed for a defined application.  
19 ReS<sub>2</sub> has the potential to make more energy efficient molecular-scale digital processors than  
20 commonly used silicon (Si).<sup>[14, 26]</sup> Particularly, in optoelectronic device fabrication, it is likely  
21 to overcome the limitation of the bulk Si because of its high absorption efficiencies in  
22 broadband wavelengths. It has emerged with a vision that ReS<sub>2</sub> will apparently be more  
23 **worthwhile** over isotropic TMDs from group VI for all known applications and beyond.

24 Recently there has been observed a growing interest in both fundamental and applied  
25 research related to ReS<sub>2</sub>. There has however been no review to date. Therefore a

1 comprehensive review of ReS<sub>2</sub> is timely. Here we critically analyse the fundamental  
2  
3 properties and relevant applications of ReS<sub>2</sub>.  
4

5 The manuscript is organised as follows. Following an introduction, a brief overview of  
6  
7 chemistry and electronic properties properties of ReS<sub>2</sub> is presented. Syntheses processes are  
8  
9 then compared and the pros-and-cons of each discussed. Then follows detailed analyses of the  
10  
11 fundamental of structural and physicochemical properties, and application of ReS<sub>2</sub> in various  
12  
13 settings including devices, energy generation and storage. This review has been concluded  
14  
15 with a view to understanding of possible future directions in synthesis, properties and  
16  
17 applications of ReS<sub>2</sub>.  
18  
19  
20  
21  
22  
23

## 24 **2. Chemistry and Electronic Properties of ReS<sub>2</sub>**

25 Rhenium (Re) was the last of the stable elements in the periodic table and was discovered by  
26  
27 Noddack, Tacke and Berg in 1925.<sup>[30]</sup> It is the heaviest congener of manganese but with  
28  
29 different chemistry, and closely resembles the Technetium. Early discovery of Re was as a  
30  
31 by-product of molybdenum.<sup>[31]</sup> When molybdenite is roasted in air it creates molybdenum  
32  
33 trioxide and volatile dirhenium heptoxide. This heptoxide can pass into effluent gases and flue  
34  
35 dusts and may be recovered by wet scrubbing or leaching with water. The elemental Re is  
36  
37 then isolated by selective adsorption as ReO<sub>4</sub> on an anion exchanger or by solvent extraction  
38  
39 from the aqueous extracts which finally precipitate as NH<sub>4</sub>ReO<sub>4</sub> or Re<sub>2</sub>S<sub>7</sub>. There are nine  
40  
41 oxidation states of Re possible. The fourth oxidation state Re(iv) is chemically favourable for  
42  
43 formation of stable solid compounds of Re through metal-metal bonding. Therefore, several  
44  
45 stable chalcogenides can produce by heating the Re and chalcogens (S, Se, Te) at elevated  
46  
47 temperature ca. 1000 °C. ReS<sub>2</sub> is the most stable phase in the Re-S system. It can also be  
48  
49 obtained by (i) heating KReO<sub>4</sub>, ReO<sub>2</sub> or ReO<sub>3</sub> with sulfur, (ii) pyrolysis of Re<sub>2</sub>S<sub>7</sub>, and; (iii) the  
50  
51  
52  
53  
54  
55  
56  
57  
58  
59  
60  
61  
62  
63  
64  
65

1 action of  $\text{H}_2\text{S}$  on aqueous  $\text{ReCl}_6^{2-}$  or  $\text{ReCl}_3$ . It is resistant to  $\text{HCl}$ , alkalis and alkalis sulfides,  
2  
3 but is oxidized by hypochlorite, nitric acid etc.<sup>[32]</sup>  
4

5 In  $\text{ReS}_2$ , both Re and S may undergo redox reactions (i.e. Re for reduction reaction and S  
6 for oxidation reaction). The redox reactivity involves induced internal electron transfer, and  
7  
8 the external oxidant leads to reduction of the metal centre. For instance, when the oxidant  
9  
10 (elemental sulfur in this case) is added to the  $\text{ReS}_2$  complex, the bound  $\text{S}^{2-}$  ligands can transfer  
11  
12 electrons to the metal centre.<sup>[33]</sup> The proclivity of the induced internal electron transfer  
13  
14 chemistry could play an integral role in the catalytic activity of enzymes and in heterogeneous  
15  
16 catalysis.  
17  
18  
19  
20  
21

22 The transition metal Re is a *d*-block transition metal having  $d^n$  configuration (here  
23  $n = 0 - 8$ ). Only  $d^3$  configuration is stable to be able to form compounds with chalcogen S.  
24  
25 The chalcogen S has an electronic configuration of  $[\text{Ne}] 3\text{S}^2 3\text{P}^4$  in which two of the three *p*-  
26  
27 orbitals possess unpaired electrons called lone-pair electrons. When S atoms are involved in  
28  
29 chemical bonding with Re, each S atom forms two covalent bonds with its neighbour.<sup>[34]</sup> The  
30  
31 unpaired *p*-electrons take part in making covalent bonds. Bonding within chains is covalent,  
32  
33 while bonding between chains is much weaker and generally considered to be of van der  
34  
35 Waals nature. In pristine  $\text{ReS}_2$ , the valence band maximum is constructed from the 5d orbitals  
36  
37 of Re atoms and 3p orbitals of S atoms, and the conduction band minimum is derived from  
38  
39 the 5d orbitals of Re atoms.<sup>[20, 35]</sup>  $\text{ReS}_2$  is an n-type direct bandgap semiconductor. The Fermi  
40  
41 level lies within 0.07 eV below the bottom of the conduction band.<sup>[36]</sup>  
42  
43  
44  
45  
46  
47  
48  
49  
50

### 51 **3. Synthesis and Isolation of Nanolayers**

52

53 Bulk  $\text{ReS}_2$  is a stack of decoupled monolayers. Therefore, top-down or bottom-up fabrication  
54  
55 of 2D nanostructures are energetically favorable. Current routes to synthesis of  $\text{ReS}_2$   
56  
57 nanostructures comprise mechanical exfoliation, chemical vapor deposition (CVD), and;  
58  
59  
60

1 chemical and liquid exfoliations.<sup>[23, 37-42]</sup> Two methods are used extensively in prototyping  
2  
3 ReS<sub>2</sub> monolayers for potential applications. The first consists of synthesis of bulk ReS<sub>2</sub> via a  
4  
5 halogen assisted vapor transport technique in high temperature (~ 1000 °C) followed by top-  
6  
7 down approach of mechanical and chemical exfoliation. The second consists of bottom-up  
8  
9 methods where monolayers are fabricated via a CVD technique.  
10

11  
12 The sticky-tape peeling-off nanoflakes from bulk ReS<sub>2</sub> surfaces, known as mechanical  
13  
14 exfoliation, is an established technique for preparing 2D nanosheets of ReS<sub>2</sub>. This method  
15  
16 yields the highest-quality monolayers samples and therefore could be used extensively in  
17  
18 fabricating high-performance devices and in understanding condensed-matter phenomena.  
19  
20 However, in the sticky-tape technique, it is difficult to control the layer thickness, uniformity,  
21  
22 and; large-scale production of nanosheets. To overcome problems with mechanical exfoliation,  
23  
24 soft-exfoliations techniques were tried, namely chemical exfoliation and liquid exfoliation. In  
25  
26 chemical exfoliation, ions of selected metals (mainly lithium) are intercalated between the  
27  
28 layers to ease the exfoliation. This could provide a solvent-free method to produce highly  
29  
30 controlled nanosheets of ReS<sub>2</sub>.<sup>[40]</sup> However, lithium intercalation results in negatively charged  
31  
32 nanosheets rather than desired neutral ones.<sup>[41]</sup> Chemical exfoliation also drives a phase  
33  
34 transition that necessitates subsequent thermal treatments to recover the original phase.  
35  
36  
37  
38  
39  
40  
41

42 Liquid-phase exfoliation is an alternative route to synthesise 2D nanosheets without  
43  
44 chemical exfoliation. Liquid exfoliation is a technique in which the bulk materials are  
45  
46 dissolved in a suitable solvent and sonicated for several hours. This technique is not much  
47  
48 studied for ReS<sub>2</sub> because finding a suitable solvent with approximately same surface tension  
49  
50 remains a challenge. Despite its ability to yield large quantities of nanomaterials, liquid  
51  
52 exfoliation cannot control structural thickness. Another solution-based method for producing  
53  
54 nanomaterials is isopycnic density gradient ultracentrifugation (iDGU). Recently, Kang et al.  
55  
56  
57  
58  
59  
60  
61  
62  
63  
64  
65



1 reported the exfoliation and layer-by-layer sorting of ReS<sub>2</sub> in aqueous surfactant solutions  
2  
3 using iDGU technique.<sup>[43]</sup>  
4

5 Both chemical and liquid exfoliation require extensive post-exfoliation modifications. The  
6  
7 problem of lithium intercalation and post-exfoliation modification was overcome by growing  
8  
9 a thin film of ReS<sub>2</sub> by the CVD method, followed by exfoliation of ReS<sub>2</sub> thin-films in N-  
10  
11 methyl-2-pyrrolidone (NMP) in an ultrasonication bath.<sup>[41]</sup> In CVD technique, solid  
12  
13 precursors of Re and S are heated to their vapor phases and reacted to form a large-area bulk  
14  
15 monolayer crystal in a substrate. This technique is presumed to be readily scalable and to  
16  
17 offer good reproducibility.  
18  
19  
20  
21

22 The disadvantages of CVD lie in: (i) its high temperature treatment that needs to continue  
23  
24 for several days to several weeks, and; (ii) exploiting a halogen vapor transport route using  
25  
26 Br<sub>2</sub> or I<sub>2</sub> as a transport agent. The high temperature is essential due to elevated melting point  
27  
28 (3180 °C) of Re powder. The elevated melting point of Re decreases the vapor pressure of Re,  
29  
30 and consequently, reduces the yields of ReS<sub>2</sub> significantly.<sup>[39]</sup> Instead of Re powder,  
31  
32 ammonium perrhenate (NH<sub>4</sub>ReO<sub>4</sub>) was also tried as a source of Re. <sup>[37]</sup> However a  
33  
34 controllable synthesis of ReS<sub>2</sub> with high crystal quality and uniform thickness using NH<sub>4</sub>ReO<sub>4</sub>  
35  
36 is yet to be practically realized. High valence state of Re (+7) and unwanted by-products are  
37  
38 the main reasons for poor crystal quality of NH<sub>4</sub>ReO<sub>4</sub> derived ReS<sub>2</sub>. <sup>[37]</sup> Halogen vapor  
39  
40 transport leads to unintentional background doping and alters the electrical properties of  
41  
42 materials. For example, I<sub>2</sub> vapor transport technique induced p-type doping and Br<sub>2</sub> usually  
43  
44 results in n-type doping.<sup>[44]</sup>  
45  
46  
47  
48  
49  
50

51 The superiority of CVD over other methods to grow 2D nanostructures would become  
52  
53 obvious if the elevated temperature and halogen vapor transport problems were solved. One  
54  
55 effective way to lower the synthesis temperature of ReS<sub>2</sub> is to form a eutectoid of Re with  
56  
57 another metal having low melting point. Zhang et al. worked on this issue.<sup>[38]</sup> They have  
58  
59  
60  
61

1 formed a Re-Te binary eutectic system introducing tellurium (Te) powder into Re powder.  
2  
3 Through this formation of Re-Te eutectoid the melting point was reduced to 430 °C. The  
4  
5 tellurium assisted eutectic synthesis of atomic layers of ReS<sub>2</sub> on mica support resulted in  
6  
7 large-area, highly crystalline and uniform monolayer thickness. A schematic of this synthesis  
8  
9 technique is been shown in **Figure 2**. It can be seen in the figure that large-area, highly  
10  
11 crystalline ReS<sub>2</sub> can be synthesized from vapor-vapor reaction between S and Re in the  
12  
13 temperature range of 460 to 900 °C. Mica substrate was used to grow uniform monolayer  
14  
15 ReS<sub>2</sub>. In another study, large-area epitaxial growth of ReS<sub>2</sub> on mica support at 500 to 800 °C  
16  
17 was reported using ReO<sub>3</sub> as a precursor of Re.<sup>[45]</sup> One critical disadvantage of these processes  
18  
19 is using the highly corrosive hydrofluoric acid (HF) as an etchant to delaminate the ReS<sub>2</sub> film  
20  
21 from the mica substrate. To avoid halogen vapor transport, Bhattacharya et al. proposed an  
22  
23 alternative approach titled the ‘Bridgman method’. This does not involve the use of any  
24  
25 transport agent.<sup>[23]</sup> However, the resulting method makes use of an elevated temperature  
26  
27 (1100 to 900 °C) and requires several weeks (~ 2) for successful growth of ReS<sub>2</sub>.  
28  
29  
30  
31  
32  
33  
34  
35

## 36 **4. Atomic Structure, Crystal Growth and Nanostructures**

### 37 **4.1. Atomic structure and crystal growth of ReS<sub>2</sub>**

38  
39  
40  
41 The asymmetric unit of ReS<sub>2</sub> is composed of two Re<sup>4+</sup> ions and four S<sup>2-</sup> ions. The layers of  
42  
43 sulfur atoms are hexagonally close-packed, and stacked along the *a*-axis and are nearly  
44  
45 parallel to *bc* plane of unit cell. Re atoms occupy the octahedral sites between every other  
46  
47 pairs of hexagonal-close-packed layers of sulfur atoms, where each Re atom is coordinated  
48  
49 with six sulfur atoms in octahedral geometry and each trigonal pyramidal sulfur atom is  
50  
51 bonded to three Re atoms. The Re atoms, that forms metal-metal bonds to three neighbours in  
52  
53 the layers of cations, results in the formation of Re<sub>4</sub> parallelogram which has a significant  
54  
55  
56  
57  
58  
59  
60  
61  
62  
63  
64  
65

1 impact on relative displacement of sulfur atoms within their hexagonal-close-packed  
 2 arrays.<sup>[24, 36]</sup> Unit cell parameters are shown in **Table 1**.

3  
 4  
 5 Conventional TMDs have graphene-like hexagonal crystal structure. In TMDs, metal  
 6 atoms ( $M$ ) are sandwiched between layers of chalcogen atoms ( $X$ ), giving rise to an  $MX_2$   
 7 stoichiometry. Chalcogen layers can be stacked on top of each other either as H phase, made  
 8 of original prismatic holes for metal atoms, or, as T phase, made of octahedral holes for  
 9 metals. Therefore, structural polytypism among the group VI TMDs is possible. The common  
 10 phases of group VI TMDs include 2H, 1T and 3R phases for bulk crystals, and 1H and 1T for  
 11 monolayer where the letters stand for hexagonal (H), trigonal (T) and rhombohedral (R).<sup>[46]</sup>  
 12 However, T-phases are reported to be metastable.<sup>[47]</sup> **Contrary, TMTCs with stoichiometric**  
 13 **formula  $MX_3$  (i.e.  $TiS_3$ ) crystalize in the monoclinic phase where parallel chains of trinagular**  
 14 **prisms make up sheets that are held together by vdW forces.**<sup>[7]</sup> The important feature of  $ReS_2$   
 15 when compared with the other  $MX_2$  or  $MX_3$  ( $M$ =Transition metals from group IV-VI and  
 16  $X$ =S, Se and Te) is its triclinic structure with in-plane structural, optical, electrical and  
 17 mechanical anisotropy along the crystal's [010] b-axis.<sup>[12, 48, 49]</sup>

18  
 19  
 20 Due to metal-metal bonding, the unit cell of  $ReS_2$  is doubled. This leads to a composition  
 21 of four Re and eight S atoms.<sup>[20]</sup> In  $ReS_2$  crystal,  $Re_4$  units form parallel 1D chains inside each  
 22 of the monolayers. These distort and eventually break the hexagonal symmetry (see **Figure 3**  
 23 **a, b**).<sup>[42]</sup> Unlike other TMDs (i.e.  $MoS_2$ ) that have high symmetry 1H-phase of trigonal  
 24 prismatic crystal and a  $D_{3h}$  point group symmetry or 2-layer hexagonal (2H) and three-layer  
 25 rhombohedral (3R),  $ReS_2$  has Peierls distortion from conventional 1T-phase of octahedral  
 26 crystal with a  $P1(\bar{6})$  symmetry.<sup>[36]</sup> Impacted by the Peierls distortion, the formation of Re  
 27 chains breaks the hexagonal symmetry. As a result, Re and chalcogen atoms in a unit cell are  
 28 forced out to same plane, and consequently, induce an in- and -out of plane anisotropy along  
 29  
 30  
 31  
 32  
 33  
 34  
 35  
 36  
 37  
 38  
 39  
 40  
 41  
 42  
 43  
 44  
 45  
 46  
 47  
 48  
 49  
 50  
 51  
 52  
 53  
 54  
 55  
 56  
 57  
 58  
 59  
 60  
 61  
 62  
 63  
 64  
 65

1 the lattice vectors.<sup>[50]</sup> This distinguishing crystal structure makes it attractive for diverse  
2 applications.  
3  
4

#### 5 6 **4.2. Interlayer coupling and polytypism**

7  
8 Widely used TMDs (MoS<sub>2</sub>, MoSe<sub>2</sub>, WS<sub>2</sub> and WSe<sub>2</sub>) are hexagonal whereas ReS<sub>2</sub> has triclinic  
9 symmetry in crystal structure. Each layer of ReS<sub>2</sub> resembles the 1T crystal structure with  
10 embedded 1D parallel chain of Re<sub>4</sub> clusters inside each monolayer. Each Re atom has seven  
11 valence electrons with one dangling electron in the 1T structure. The extra electrons result in  
12 strong covalent bonding between Re atoms. Formation of Re-Re covalent bonding impacts the  
13 energy balance of the system, acoustic phonons and the lattice structure. Influenced by the  
14 covalent bonding, the lattice becomes a distorted 1T structure wherein Re atoms in the layer  
15 form a zig-zag Re-Re chain (**Figure 4**).<sup>[13, 51, 52]</sup> Because of the presence of Re chain inside  
16 each layer, energy difference of ReS<sub>2</sub> layers when sliding from one layer to other becomes  
17 very nominal and therefore lacks order in stacking. In addition, one extra electron on the Re  
18 atoms results in significantly less intra-layer polarization and weakens the van der Waals  
19 interaction in interlayer. The lack of ordered stacking and the weak intra-layer polarization are  
20 the overriding reasons behind the vanishing interlayer coupling of ReS<sub>2</sub> layers.<sup>[20]</sup> However,  
21 the existence of lacked interlayer coupling was put into debate when several groups reported  
22 the existence of polytypism and strong interlayer coupling in ReS<sub>2</sub> layers.<sup>[53-55]</sup> More  
23 extensive study is needed to resolve this.  
24  
25  
26  
27  
28  
29  
30  
31  
32  
33  
34  
35  
36  
37  
38  
39  
40  
41  
42  
43  
44  
45  
46

#### 47 **4.3. Growth mechanism of nano-architectures of ReS<sub>2</sub>**

48 Assembly of nanoscale building blocks into functional nanostructured materials has a strong  
49 impact on the promotion of rapid development of nanoscience and nanotechnology.  
50 Significant research efforts have therefore been made in the past to mimic shapes and  
51 structures that exist in nature. Different nano-architectures of ReS<sub>2</sub> have been under  
52  
53  
54  
55  
56  
57  
58  
59  
60

1 investigation.<sup>[42], [56, 57]</sup> Below we discuss the recently reported ReS<sub>2</sub>-derived nanostructures  
2  
3 and related growth mechanisms.  
4

5 Hafeez et al. explained the growth mechanism of nano-rod and sheet-like ReS<sub>2</sub> in CVD  
6  
7 technique (*see* **Figure 3 c-f**).<sup>[42]</sup> There are two growth directions, (100), which is fast and  
8  
9 dominant, and; (020) which is relatively slow. This asymmetry of directional growth ideally  
10  
11 culminates with nanorods-like 1D structure. To form a sheet-like hexagonal structure, the  
12  
13 growth rate in both directions must be comparable. This can be achieved by varying the  
14  
15 concentration of carrier gases (N<sub>2</sub> and H<sub>2</sub>). It was shown that for N<sub>2</sub>:H<sub>2</sub> = 10:1 and N<sub>2</sub>:H<sub>2</sub> =  
16  
17 2:1, growth of nanorods and hexagons of ReS<sub>2</sub>, respectively, were obtained. Greater  
18  
19 concentrations of H<sub>2</sub> decreases the planar density through introducing sulfur vacancies, and  
20  
21 increases the number of unpaired bonds and energy of the plane that reduces the growth rate  
22  
23 of the plane. At some points, growth rate of (100) plane become comparable to that of (020)  
24  
25 plane and the growth of hexagonal flake of ReS<sub>2</sub> commenced.  
26  
27  
28  
29  
30  
31

32 Conventional 2D materials e.g. graphene have strong interlayer coupling for which  
33  
34 nanosheets are stacked in face-to-face orientation. Due to the strong van der Waals (vdW)  
35  
36 forces, graphene sheets tend to aggregate and form graphite to minimize the surface free  
37  
38 energy. As a result, the face-to-face assembly of nanosheets culminates with poor surface area  
39  
40 and kinetic ion transport. Therefore, edge-to-edge assembly is highly desirable. For self and  
41  
42 edge-to-edge assembly, interlayer coupling of 2D material should be weak. Fortunately,  
43  
44 layers of ReS<sub>2</sub> are coupled with each other by extremely weak vdW forces that allow two  
45  
46 tangent ReS<sub>2</sub> nanoflakes to slide near without friction. Taking the anisotropic and weak  
47  
48 interlayer coupling into consideration, Zhang et al. reported self-assembled nanoflakes and  
49  
50 nanoscrolls of ReS<sub>2</sub> using electrochemical lithium intercalation process.<sup>[56]</sup> These authors have  
51  
52 discussed four possible routes to grow from the nanoflakes to nanoscrolls (*see* **Figure 5**).  
53  
54  
55  
56  
57  
58  
59 Firstly, adjacent nanoflakes stack face-to-face. Secondly, randomly distributed nanoflakes  
60  
61  
62  
63  
64  
65

1 retain their disordered structure. Thirdly, pre-existing nanoflakes tend to slide away  
2  
3 influenced by the combined anisotropic and electrostatic forces. Finally, nanoflakes with  
4  
5 coherent facets approach and then fuse together to turn into nanoscrolls.  
6

#### 7 8 **4.4. Architecture and orientation of domain and grain boundaries** 9

10 The isotropic nature of group VI-TMDs facilitates the crystalline growth mode with well-  
11 defined domain architecture and grain boundaries. In contrast, ReS<sub>2</sub> is anisotropic. Because of  
12 this anisotropy interfacial energy, it stabilizes the dendritic growth mode but prevents well-  
13 defined crystalline orientation. Therefore, an understanding of the growth-mechanisms of  
14 domain architecture and grain boundaries is crucial for: (i) successful synthesis of highly  
15 crystalline ReS<sub>2</sub> monolayer with noteworthy structural anisotropy, and; (ii) in gaining insight  
16 into how subdomains arrange themselves to build large-scale flakes, and in which direction  
17 Re-chains are oriented within each subdomain.  
18  
19  
20  
21  
22  
23  
24  
25  
26  
27  
28  
29

30 Due to strong interaction and dimerization between adjacent Re-atoms, highly oriented Re-  
31 Re chain forms in ReS<sub>2</sub> along the lattice direction of *b*-axis. **Figure 6a** illustrates the  
32 molecular Re-Re chain in [010] direction of *b*-axis. When Re-Re chains coalesce at different  
33 approaching angles, clusters of vacancy related defects evolve that alter the direction and  
34 rotation of Re-chains around the *b*-axis.<sup>[58]</sup> In this, several types of domains e.g. triangular,  
35 hexagonal etc., can be formed depending on flow rate, temperature and precursors. During  
36 growth of nucleation sites, when two or more domains meet, a grain boundary is formed.  
37  
38  
39  
40  
41  
42  
43  
44  
45  
46

47 It was demonstrated through angle-resolved Raman intensity mapping that the flakes of  
48 hexagonal domains are not made of randomly oriented Re-Re chains along *b*-axis, but are  
49 made of subdomains.<sup>[58]</sup> Within hexagonal domains, subdomains are triangular. **Figure 6b**  
50 illustrates the Raman intensity mapping at 214 cm<sup>-1</sup> peak (because intensity of 214 cm<sup>-1</sup> mode  
51 reaches a maximum when the polarization vector is nearly parallel to the *b*-axis lattice  
52 direction. The vibrational origin of this peak is related to in-plane vibrations of Re-atoms<sup>[16, 21,</sup>  
53  
54  
55  
56  
57  
58  
59  
60  
61  
62  
63  
64  
65

<sup>54]</sup>) at different polarization angles from  $0^\circ$  at  $60^\circ$  steps. It was shown (**Figure 6b**) that the direction of Re-chain is closely aligned for subdomains located  $180^\circ$  position apart. The domains form grain boundaries when running from about  $30^\circ$  to  $210^\circ$ ,  $90^\circ$  to  $270^\circ$ , and;  $150^\circ$  to  $330^\circ$ . This is highlighted (red lines) in **Figure 6c** where A, B, C, D, and F denote triangular subdomains. It was concluded that opposite triangular domains (A-D, B-E, and C-F) have similar *b*-axis orientation. On the other hand, in truncated triangular flakes, Re-chains directions are oriented toward  $90^\circ$ ,  $330^\circ$  and  $210^\circ$ , respectively. This implies that Re-chains are randomly oriented in close proximity to grain boundaries for which *b*-axis within each subdomain orients perpendicular to the truncated edge.

The formation of grain boundaries in other 2D materials such as graphene, h-BN and MoS<sub>2</sub> are well defined. For example, grain boundaries in graphene are formed by dislocations originating from 5-7 carbon rings and by different carbon vacancies<sup>[59]</sup>, whilst in h-BN and MoS<sub>2</sub>, it is due to the 4l6, 4l8, 5l5, and 6l8 B-N and Mo-S rings.<sup>[60]</sup> Unlike these 2D materials the elucidation of formation of grain boundaries in ReS<sub>2</sub> is not clear - due to anisotropy in the interfacial energy and number of different atomic arrangements around defect sites.<sup>[50]</sup>

## 5. Fundamental Properties

ReS<sub>2</sub> is one of the least known among transition metal dichalcogenides. However, it is by no means a typical transition metal dichalcogenide, rather it has distinctive properties that are less common in popular TMDs. Firstly, it consists of Re which is an heavier element than any other TMDs, and therefore, exhibits high spin-orbit interaction. Secondly, the unit cell is also relatively large, asymmetric, and the surface is corrugated on the lateral length of its unit cell. Further, its monolayer is highly anisotropic and contains both metal-metal and metal-chalcogen bonds.<sup>[16, 25, 61]</sup> Owing to its unusual atomic structure and assymetric crystal growth,

1 ReS<sub>2</sub> exhibits different fundamental properties from other TMDs. Here below we have  
2  
3 reviewed such properties.  
4

## 5.1 Vibrational properties

5  
6  
7  
8 Lattice vibrations play a crucial role in the intriguing properties and observed phenomena in  
9  
10 layered 2D ReS<sub>2</sub>. The inter-layer interaction of vdW structures facilitate the lattice vibration  
11  
12 and evolution of different phonon modes (such as shear and breathing phonons). Raman  
13  
14 spectroscopy is a nondestructive and generally used technique to elucidate all phonons modes.  
15  
16 An understanding of the vibrational properties enable identification of the structure, lattice  
17  
18 symmetry, crystal quality, existence of defects, and; impurities etc., which in turn could  
19  
20 provide key information about the mechanical, thermal, electronic and optical  
21  
22 properties.<sup>[28, 47, 62]</sup>  
23  
24  
25  
26

### 5.1.1 Raman spectroscopy for probing 2D ReS<sub>2</sub>

27  
28  
29 There are two types of active Raman modes in 2D ReS<sub>2</sub>, such as intralayer vibration modes  
30  
31 and interlayer vibration modes.<sup>[20, 62]</sup> Intralayer vibration modes appear usually in higher  
32  
33 frequencies. The interlayer vibration mode is sub-divided into shear modes and breathing  
34  
35 modes, and usually appears at lower (< 50 cm<sup>-1</sup>) frequencies. To observe these lower  
36  
37 frequency vibrational modes is quite challenging.  
38  
39  
40  
41  
42

43  
44 The experimental observation of a particular phonon mode in Raman spectroscopy  
45  
46 depends on symmetry selection rules and scattering geometry. A detailed knowledge of  
47  
48 Raman tensor, group theory analysis, and; materials space group is essential to understand  
49  
50 how Raman spectroscopy actually works. The number of brillouin zone centre ( $\Gamma$ ) phonons  
51  
52 for given 2D material is equal to the three times that of the number of atoms in a unit cell.<sup>[47]</sup>  
53  
54 The  $\Gamma$ - point phonons are a combination of acoustic and optical modes, and not all the  
55  
56 phonons are Raman active. For example, A  $MX_2$  with  $D_{6h}$  point group symmetry and a unit  
57  
58  
59  
60



cell consists of 6 atoms will have 18 phonons modes which could be described as  $\Gamma = A_{1g} + 2A_{2u} + E_{1g} + 2E_{1u} + 2E_{2g} + E_{2u} + 2B_{2g} + B_{1u}$ . Among these 18 modes,  $A_{1g}$ ,  $E_{1g}$  and  $2E_{2g}$  are Raman active.<sup>[28]</sup>

### 5.1.2 High frequency vibrational modes in $ReS_2$

The unit cell of  $ReS_2$  consists of 12 atoms (4 Re atoms and 8 S atoms). Therefore, it will have 36 vibrational modes and 36  $\Gamma$ -point phonon modes that can be written as  $\Gamma = 18(A_g + A_u)$ . Among these 36  $\Gamma$ -point phonon modes, 18  $A_u$  modes consist of three acoustic and 15 infrared optical modes which are asymmetric and inactive in Raman spectroscopy.<sup>[62]</sup> This implies that there are only 18 Raman modes that can be found in  $ReS_2$  (see **Figure 7 a, b**). The frequencies of these 18 Raman active modes are listed in **Table 2**, where  $A_g$  represent out-of-plane vibrational mode,  $E_g$  in-plane vibrational mode and  $C_p$  in-plane and out-of-plane coupled mode. While there are some degenerate modes exist for other  $MX_2$ , all of the Raman active and inactive modes in  $ReS_2$  are nondegenerate.

There are 4 out-of plane vibrational modes, 6 in-plane vibrational modes and 8 coupled modes recorded for  $ReS_2$ . The out-of plane modes located at 136.8 and 144.5  $cm^{-1}$  are assigned to out-of-plane vibrations of Re atoms, whilst the modes at 422.3 and 443.4  $cm^{-1}$  are for the out-of-plane vibrations of S atoms. Among the in-plane modes, the modes at 153.6, 163.4, 218.2 and 238.1  $cm^{-1}$  are caused by the in-plane vibrations of Re atoms, while the modes at 308.5 and 312.1  $cm^{-1}$  are due to the in-plane vibrations of S atoms. The  $C_p$  modes are a mix of in-plane and out-of-plane vibrations of Re and S atoms.<sup>[20, 62]</sup>

As can be seen in **Figure 7b**, the difference in Raman shifts between bulk to monolayer is tiny. This suggests an ultra-weak interlayer interaction, and implies that the monolayer could behave like a vibrationally decoupled bulk  $ReS_2$ .<sup>[20, 62]</sup>

### 5.1.3 Low frequency vibrational modes in ReS<sub>2</sub>

ReS<sub>2</sub> exhibits rich low-frequency Raman spectra. There are three pronounced Raman peaks at 13, 16.5 and 28 cm<sup>-1</sup> observed for two-layer ReS<sub>2</sub> (see **Figure 7c**).<sup>[53, 54]</sup> However, these peaks are absent in monolayer, implying that the peaks originated from the vibrations between the two layers.<sup>[55]</sup> The Raman peak at 28 cm<sup>-1</sup> was assigned to breathing mode, while the peaks at 13 and 16.5 cm<sup>-1</sup> were assigned to parallel shear modes (S<sub>||</sub>) and vertical shear modes (S<sub>⊥</sub>), respectively. These interlayer modes in ReS<sub>2</sub> are more distinctive than other 2D materials. Notably, the shear modes in ReS<sub>2</sub> is nondegenerate while they are degenerate for other 2D materials. Additionally, the breathing mode is stronger than shear modes in ReS<sub>2</sub>, whereas the shear modes are stronger than breathing modes in other 2D materials.

The emergence of interlayers phonon modes indicates significant lattice coupling between the ReS<sub>2</sub> layers. In particular the observation of the shear modes indicates a well-defined layer stacking order in ReS<sub>2</sub> crystal.<sup>[21, 53-55]</sup> This is because generation of shear mode vibrations require good atomic registration between neighbouring layers.

## 5.2 Band structure and electronic transport

ReS<sub>2</sub> is a direct gap diamagnetic semiconductor. Its valence band and conduction band edges are composed of *d*-orbital of Re atoms and *p*-orbitals of S atoms.<sup>[20]</sup> As shown in **Figure 8a**, the band structure of mono-, tri- and penta- layers ReS<sub>2</sub> calculated by *ab initio* method shows the nature of direct band gap without any direct-to-indirect transition.<sup>[26]</sup> Moreover, the overall bandgap doesn't change significantly from mono-layer to multi-layers. The room temperature Hall mobility of n-type ReS<sub>2</sub> and the impurity carrier activation energy was reported to be 19 cm<sup>2</sup> V<sup>-1</sup> and 178 meV, respectively.<sup>[63]</sup>

Due to charge decoupling from an extra valence electron of Re-atoms, ReS<sub>2</sub> crystallizes in a distorted 1T diamond-chain structure. This distortion in crystal structure renders weak coupling between interlayers which can result in the bulk ReS<sub>2</sub> behaving like electronically

1 and vibrationally decoupled monolayers.<sup>[16, 20, 64]</sup> This is a significant advantage over other  
2  
3 TMDs which undergo a transition from indirect to direct bandgap semiconductor when  
4  
5 reduced from bulk to monolayer. The resilient bandgap with no direct-indirect transition  
6  
7 offers remarkable possibilities to produce relatively large-area ReS<sub>2</sub> of a single molecular  
8  
9 layer thickness. Both the monolayer and bulk ReS<sub>2</sub> is a direct gap semiconductor with a  
10  
11 bandgap of ~1.55 eV for monolayer and 1.47 for bulk, respectively.<sup>[35, 65]</sup>  
12  
13  
14

15 In ReS<sub>2</sub> (i) overlapping of electron wavefunctions from adjacent layers is so weak that a  
16  
17 modulation of the interlayer distance cannot renormalize the band structure, implying that  
18  
19 ReS<sub>2</sub> is electronically decoupled, (ii) whilst other TMDs in transition from bulk to monolayer  
20  
21 exhibit a crossover from indirect to direct bandgap, the thinning down of ReS<sub>2</sub> does not alter  
22  
23 its bulk-phase direct bandgap, and; (iii) whilst other TMDs are prone to out-of-plane quantum  
24  
25 confinement with decreasing thickness, quantum confinement in ReS<sub>2</sub> is virtually independent  
26  
27 of number of layers (because neighbouring monolayers in the flake are largely electronically  
28  
29 decoupled, thinning down the flake does not enhance the quantum confinement of electrons in  
30  
31 the system; this is evidence for the optically decoupled nature of ReS<sub>2</sub>).<sup>[5, 18, 20, 49, 53-55, 62, 66, 67]</sup>  
32  
33  
34  
35  
36

37 The intrinsic carrier mobility and resistivity of ReS<sub>2</sub> depends on temperature and electron  
38  
39 density.<sup>[68]</sup> Carrier mobility is inversely related to temperature. Therefore ReS<sub>2</sub> exhibits  
40  
41 semiconductor-to-metallic behaviour at high electron densities and low temperatures.<sup>[69]</sup> This  
42  
43 is because at high densities of electrons resistivity decreases significantly. The metallic state  
44  
45 of ReS<sub>2</sub> is a result of second-order metal-to-insulator transition driven by electronic  
46  
47 correlation. This result is indicative of the susceptibility of band structure of ReS<sub>2</sub> to applied  
48  
49 electric-fields. This feature of semiconductor-metal transition could open significant  
50  
51 technological possibilities in electronics and optoelectronics where the same material can be  
52  
53 used as both semiconducting channel and metallic interconnects.  
54  
55  
56  
57  
58  
59  
60  
61  
62  
63  
64  
65

1 The bandgap and electronic transport (i.e. effective mass, mobility etc.) of ReS<sub>2</sub> can also be  
2 modulated by applying appropriate strain in three directions *a*, *b* and *c* of unit cell. It has been  
3 demonstrated that tensile strain lowers the conduction band minimum (VBM) and raises the  
4 valence band maximum (VBM) resulting in a reduced bandgap. The strain can change  
5 significantly the effective mass as well as the mobility of hole, while it has relatively small  
6 impact on the effective mass and mobility of the electron. For example, *a*-direction strain  
7 increases the hole effective mass but decreases hole mobility. Whilst *b*-direction strain  
8 decreases the hole effective mass, but increases the hole mobility.<sup>[67]</sup> This directional change  
9 of electronic transport in ReS<sub>2</sub> could be used to make a strain-sensor.

### 5.3 Excitonic and absorption properties

24 A monolayer of group VI transition metals (MoS<sub>2</sub>, MoSe<sub>2</sub>, WS<sub>2</sub> and WSe<sub>2</sub>) has high crystal  
25 symmetry. Therefore, these exhibit isotropic linear properties of optical absorption and  
26 emission. In contrast ReS<sub>2</sub> has reduced crystal symmetry which gives rise to anisotropic in-  
27 plane optical properties.<sup>[21, 51, 70-72]</sup> Research related to the electron-electron and hole-hole  
28 interactions in the excited state concluded that the anisotropic optical absorption on ReS<sub>2</sub> was  
29 due to strongly bound excitons. The triclinic crystal structure of ReS<sub>2</sub> leads to polarization  
30 dependent optical absorption.<sup>[65]</sup> The anisotropic absorption coefficient and transient  
31 absorption was maximum when the light polarization was parallel to the Re chains, and  
32 minimum when perpendicularly polarized.<sup>[72]</sup> Many-body perturbation theory computations  
33 have shown that the lowest-energy bright excitons of distorted 1T ReS<sub>2</sub> exhibit a perfect  
34 figure-eight shape polarization - which is unusual for hexagonal TMDs. As a result, ReS<sub>2</sub> is  
35 active in capturing photons within near-infrared frequency regimes and is therefore expected  
36 to be useful for optoelectronic applications.<sup>[73]</sup>

37 Apart from absorption anisotropy, photoluminescence (PL) emission spectra show  
38 significant difference with that of conventional TMDs. For group VI TMDs, the emission  
39

1 intensity is increased in monolayer by an order of magnitude compared with the bulk due to  
2 crossover from indirect to direct band gap transition. In contrast, intensity increases with  
3 number of layers in  $\text{ReS}_2$  (see **Figure 8b**). In the optical absorption spectra, three optical  
4 transitions were identified for both bulk and monolayer  $\text{ReS}_2$ , indicating decoupled excitonic  
5 and emission properties.<sup>[70]</sup>

#### 12 **5.4 Impact of vacancies on electronic and magnetic properties**

13 In addition to 1T-distorted crystal structure, the formation of imperfections e.g. point defects,  
14 grain boundaries etc., significantly influence the electronic, optical, mechanical and magnetic  
15 properties of  $\text{ReS}_2$ . Imperfections are induced due to the synthesis and transfer procedure  
16 during crystal growth, or exfoliation from bulk-to-monolayer. Existence of lattice  
17 imperfections create localized electronic and excitonic states which can alter the optical  
18 absorption, charge carrier generation, separation and transportation dynamics.

19 With  $\text{ReS}_2$ , formation of sulfur (S) and Re vacancies are very likely to happen. The most  
20 commonly observed vacancies (also known as point defects) are: monosulfur vacancies ( $V_s$ ),  
21 disulfur vacancies ( $V_{2s}$ ), two monosulfur vacancies ( $V_{s+s}$ ), Re vacancy ( $V_{\text{Re}}$ ), complex of Re  
22 and monosulfur/disulfur ( $V_{\text{Res}}, V_{\text{ReS}_2}$ ), and; sulfur substituted Re vacancies ( $S_{s \rightarrow \text{Re}}; S_{2s \rightarrow \text{Re}}$ ).<sup>[50]</sup>

23 The relative stability of these point defects depends on the formation energy within an  $\text{ReS}_2$   
24 supercell. The defect formation energies as a function of sulfur chemical potential, illustrated  
25 in **Figure 9**, have been adopted from the work of Horzum et al.<sup>[50]</sup> Among the stated point  
26 defects, monosulfur vacancy is energetically more favorable and therefore likely to occur.  
27 This is because it has the lowest formation energy. Sulfur vacancies could result in  
28 nonmagnetic semiconducting ground states. In contrast, Re vacancies could lead to spin  
29 polarized ground states with localized magnetic moments of  $1 - 3 \mu_B$ ; but are less likely to  
30 happen as large amounts of energy are required to create an Re vacancy. It should be noted  
31 that in cases of co-existence of sulfur and Re point defects, these however, do not annihilate

1 the semiconductor nature of ReS<sub>2</sub> - except a slight change in the bandgap. The amount of  
2  
3 change in intrinsic bandgap of 1.47 to 1.27 or 1.08, eV depends on the mono or disulfur  
4  
5 vacancies, respectively, that are created within the lattice structure.  
6

### 7 8 **5.5 Doping influenced electrical, optical and magnetic properties** 9

10 Doping is generally used as a practical way to achieve custom-made changes in  
11  
12 physicochemical properties. It is widely accepted that when an intrinsic semiconductor is  
13  
14 shown to be ineffective for desired applications, the introduction of foreign atoms by means  
15  
16 of doping is feasible to modulate intrinsic electronic, optical and magnetic properties.  
17  
18

19  
20 For ReS<sub>2</sub> introduction of metal/non-metals foreign atoms as dopants can be accomplished  
21  
22 through substitution of S or Re atoms. Among the metals/non-metals in the periodic table, Cl  
23  
24 was reported as the more ideal candidate for n-type doping and Mo, P as ‘best candidates’ for  
25  
26 p-type doping of ReS<sub>2</sub> monolayer.<sup>[74]</sup> It was demonstrated that doping can increase electrical  
27  
28 conductivity through increasing the carrier density. Loh et al. have reported that fluorination  
29  
30 can be used to tailor electronic and magnetic properties of ReS<sub>2</sub>.<sup>[75]</sup> They reported that F  
31  
32 atoms above the Re chains could induce ferromagnetically coupled metallic mid-gap states  
33  
34 within the Re chains but antiferromagnetically coupled between the Re chains. However, F  
35  
36 atoms between the Re chains induced semiconducting mid-gap states and therefore are non-  
37  
38 magnetic. Fluorinated ReS<sub>2</sub> therefore looks promising for spintronic and spin-wave logic  
39  
40 devices. The net magnetic moment of doped ReS<sub>2</sub> varies between  $0 < \mu_B \leq 1$ .<sup>[74]</sup> A red-shift in  
41  
42 optical absorption was observed for Nb doping of ReS<sub>2</sub>, however, the direct band-edge  
43  
44 excitonic transition energies remain practically unchanged.<sup>[76]</sup> The absorption-edge anisotropy  
45  
46 of ReS<sub>2</sub> crystal makes it a promising material for fabrication of polarization sensitive  
47  
48 photodetectors. Such a detector was demonstrated in multichannel optical communication for  
49  
50 detecting various orientations of linearly polarized light.<sup>[71, 77]</sup>  
51  
52  
53  
54  
55  
56  
57  
58  
59  
60  
61  
62  
63  
64  
65

## 5.6 Modulation of electrical, optical and magnetic properties by adatoms adsorption

In addition to doping and defects-induced changes in electro-optical-magnetic properties, adsorption of adatoms could also be used to tune these properties.<sup>[78]</sup> Adatoms are chemically adsorbed atoms on the surface of given material. On adsorption of an adatom, charge transfer between the adatom and the host material is the key in accessing unusual electronic, magnetic and optical properties of the host material.<sup>[10, 79]</sup> Adsorption of adatoms is governed by the electronegativity of the adatoms, atomic distance between the adatom and substrate, and the states of the surface of the host material.<sup>[10, 35, 80]</sup>

Unlike other TMDs, ReS<sub>2</sub> shows stronger interaction between non-metal adatoms (H, N, P, O, S, F etc.) due to softer Re-S bonding.<sup>[35, 81]</sup> The preferential sites for non-metal adatoms adsorption in ReS<sub>2</sub> are peak and valley sites of sulfur (S) atoms. With the exception of H, all other non-metal adatoms adsorption can maintain the semiconductor nature of ReS<sub>2</sub>. H adsorption pulls the Fermi level into the conduction band and results in a semiconductor-metal transition. N and P adsorption bring spin polarized defect states in the gap, resulting in a half-semiconducting feature. It has been shown that it is possible to achieve metal-free magnetism with a long-range magnetic coupling interaction at low defect concentrations and a tunable bandgap.<sup>21</sup> In traditional cases, the magnetic moment arises from the d-electrons of transition-metal atoms, but the magnetism based on the sp states of non-metal elements is the reason behind achievement of metal-free magnetism in ReS<sub>2</sub>. This metal-free magnetism has strong coupling interactions with noclustering effect of magnetic ions.<sup>[82]</sup> These properties are highly desirable to fabrication of electronic and spintronic devices based on ReS<sub>2</sub>.

## 6. Applications

The anisotropy of its structural, physical and fundamental properties makes ReS<sub>2</sub> a good choice for exploring applications in a variety of settings. New applications of ReS<sub>2</sub> appear

1 almost every day, pushing its usability horizon further. However, most applications of ReS<sub>2</sub> to  
2  
3 date are confined to electronic-optoelectronic device fabrication, energy storage and catalytic  
4  
5 hydrogen production. These applications are reviewed below.  
6

### 7 8 **6.1. Electronic and optoelectronic device fabrication** 9

10 Solid state devices, such as field effect transistors (FET) and optoelectronics (photodetector,  
11  
12 photodiode, phototransistors etc.) have had a revolutionary impact on forming the modern  
13  
14 world.<sup>[12]</sup> They are the basic building blocks of systems in modern information and  
15  
16 communications technology (ICT). Silicon has dominated applications in solid state devices  
17  
18 fabrication. Whilst devices need scaling down from micro- to nano- level, silicon imposes  
19  
20 serious restrictions because it is not a layered material.<sup>[1, 2]</sup> Researchers are trying to find new  
21  
22 materials beyond silicon for solid-state device fabrication. The rise of graphene in 2004 came  
23  
24 with expectations that it might be a better material than silicon for fabrication of noble  
25  
26 electronic devices.<sup>[1]</sup> However, it is now clear that graphene will not meet these expectations  
27  
28 as it lacks a bandgap which is needed for FET, and other optoelectronic device operation.<sup>[83]</sup>  
29  
30 Since 2011 the International Technology Roadmap for Semiconductors (ITRS) has discussed  
31  
32 2D materials ‘beyond’ graphene as candidates for future electronics.<sup>[84]</sup> TMDs, in this regards,  
33  
34 evolved as alternative candidate materials beyond silicon because of their unique monolayer  
35  
36 and few-layers electronic properties. Apart from popular TMDs (e.g. MoS<sub>2</sub>, MoSe<sub>2</sub>, WS<sub>2</sub>,  
37  
38 WSe<sub>2</sub>)<sup>[18, 85, 86]</sup>, ReS<sub>2</sub> as a newly explored TMD has attracted significant attention as a material  
39  
40 for solid state device applications.  
41  
42  
43  
44  
45  
46  
47  
48

49 In recent years, ReS<sub>2</sub> has found application in fabrication of electronic and optoelectronic  
50  
51 devices, such as thin film transistors (TFT), digital logic devices and photodetectors.<sup>[18, 26, 27, 64,  
52  
53 69, 87-93]</sup> For example, Shim et al.<sup>[91]</sup>, Corbet et al.<sup>[87, 92]</sup> and Liu et al.<sup>[27]</sup> reported ReS<sub>2</sub>-based  
54  
55 TFTs with high on/off current ratio of 10<sup>7</sup>, 10<sup>4</sup> and 10<sup>5</sup>, respectively, and Zhang et al.<sup>[89]</sup> and  
56  
57 Liu et al.<sup>[27]</sup> demonstrated ReS<sub>2</sub>-based photodetectors with a photoresponsivity of  
58  
59  
60



1 88600 and  $16.14 \text{ A W}^{-1}$ , respectively. Prototypes of  $\text{ReS}_2$  based FET, photodetector and  
2  
3 digital inverter are shown in **Figure 10**. For detailed synthesis procedures, the Readers is  
4  
5 directed to the references mentioned in the caption of the **Figure 10**.  
6

7  
8 The short-channel effects set a limit to the miniaturization of intensively used metal-oxide-  
9  
10 semiconductors (MOS) in FET devices fabrication.<sup>[94]</sup> Ultrathin 2D materials appeared as a  
11  
12 viable solution to overcome the scaling-down problem of MOSFET.<sup>[95]</sup> Like other TMDs,  
13  
14 atomically thin  $\text{ReS}_2$  has drawn significant interest for device fabrication, particularly in FET,  
15  
16 because of its ability to eliminate drain induced short-channels effects.<sup>[12, 96]</sup> In addition,  
17  
18 atomically smooth surfaces of  $\text{ReS}_2$  are void of dangling bonds which can significantly reduce  
19  
20 the interface state densities and abate the surface roughness scattering.<sup>[87]</sup>  
21  
22

23  
24  
25 With  $\text{ReS}_2$  bandgap always remains direct irrespective of bulk to single layers transition as  
26  
27 a result of charge decoupling from an extra valence electron in the Re atoms - which causes it  
28  
29 to take a distorted 1T crystal structure. It should be noted that other TMDs undergo a direct to  
30  
31 indirect transition when the number of layers decreases. This difference between  $\text{ReS}_2$  and  
32  
33 other TMDs makes  $\text{ReS}_2$  more appealing for optoelectronics and interband tunnel FET where  
34  
35 a direct bandgap is required to maintain efficient photon absorption-emission and electron  
36  
37 transmission, respectively. Therefore,  $\text{ReS}_2$  is anticipated as a future seamless platform in  
38  
39 which logic FETs could be combined with optoelectronic devices.  
40  
41  
42

43  
44 Integrated circuits control the so called “digital” world. The more complex the system  
45  
46 requirements the greater the number of integrated devices. A modern computer chip (with an  
47  
48 approx. area of one inch square) which that consists of billions of transistors is a good  
49  
50 example of a typical complex integrated circuit. For instance, processors contained five-  
51  
52 billion MOSFETs with gate lengths around 20 nm from 2014, and 10-billion of such  
53  
54 processors were commercially available in 2015.<sup>[84]</sup> There are two demands in integrated  
55  
56 circuit design, one is large-scale integration in a limited confined space, and; the other is  
57  
58  
59  
60

1 reduced-power consumption to drive the circuit. For leading complementary metal-oxide-  
2 semiconductor (CMOS) technologies, scalability ( $< 10$  nm) and large-integration with  
3 optimized performance is a significant challenge - even after tailoring material properties and  
4 circuit design variables.<sup>[12, 96, 97]</sup> In contrast to CMOS technologies, researchers are trying to  
5 find solutions in lattice oriented tuning of transport properties, and optimization of circuit  
6 performance for future 2D integrated circuits.<sup>[98]</sup> In keeping with this anisotropic ReS<sub>2</sub> could  
7 become the material of choice for integrated circuits in the future. In fact, Liu et al. have  
8 demonstrated a logic inverter circuit by fabricating two FETs on a 60° angle quadrilateral-  
9 shaped ReS<sub>2</sub> flakes.<sup>[26]</sup> This inverter was shown to have a voltage gain, a measure of  
10 sensitivity, larger than unity. This is essential for cascading multiple inverter toward more  
11 complex systems design. ReS<sub>2</sub> therefore shows significant promise for both single device  
12 fabrication, and more complex integrated circuit design.

13 This is true particularly in transistor applications where any new material should meet the  
14 following criteria: (i) a room temperature bandgap of 400 meV, is needed for good switch-off  
15 and on-off ratios, (ii) faster carrier transport with low effective mass - because the speed of  
16 the carrier transport is mobility and mobility inversely proportional to carrier effective mass,  
17 (iii) high thermal conductivity to avoid self-heating, (iv) low contact resistance for improved  
18 channel conductivity, and; (v) ability to suppress undesirable short-channel effect whilst  
19 scaling down to nanometer scale. ReS<sub>2</sub> is amenable to most of these criteria. Therefore, it is  
20 anticipated that ReS<sub>2</sub> might become the next material for electronic and optoelectronic device  
21 fabrication.

## 22 **6.2. Energy storage**

23 Rechargeable batteries, such as lithium ion batteries (LIBs), are eco-friendly power sources  
24 for portable electronics, power tools and vehicles. These are increasingly popular because of  
25 their greater energy density, better rate capability and longer cycling life.<sup>[99]</sup> The rate

1 determinant for efficiency of LIBs is related to rapid diffusion of lithium ions.<sup>[100]</sup> TMDs have  
2 larger interlayer spacing, higher specific capacity and better recycling behaviour than graphite.  
3 Therefore, layered TMDs have shown greater efficiency over commercially-used graphite as  
4 an anode for LiBs application.<sup>[101]</sup>  
5  
6  
7  
8  
9

10 ReS<sub>2</sub> is in many ways significantly different from other TMDs. It is characterized by  
11 absence of band renormalization, identical behaviour to bulk materials and monolayers, weak  
12 interlayer coupling (18 mV vs. 460 mV per unit cell for MoS<sub>2</sub>), and; greatest anisotropic ratio  
13 (along two principle axes) among the 2D layered materials.<sup>[18, 20, 26, 93]</sup> Moreover, ReS<sub>2</sub>  
14 exposes more active sulfur edges which can provide ready intercalation and deintercalation of  
15 lithium.<sup>[102]</sup> These characteristics of ReS<sub>2</sub> facilitate the massive lithium ions to efficiently  
16 diffuse without significant volume expansion This is a highly significant advantage over other  
17 2D layered materials.<sup>[21, 103]</sup> As a result, ReS<sub>2</sub> appears to possess significant potential in high-  
18 current density LIBs. A 430 mAh g<sup>-1</sup> of lithium storage capacity has been reported for ReS<sub>2</sub>.  
19 This storage capacity has been improved to 1000 mAh g<sup>-1</sup> by coupling graphene into the ReS<sub>2</sub>  
20 framework in a 3D fashion.<sup>[102]</sup> Graphene incorporation increases the conductivity and  
21 specific surface area and shortens the pathways and facilitates fast diffusion of both lithium  
22 and electrolyte ions. A schematic illustration of lithium intercalation in graphene supported  
23 ReS<sub>2</sub> and improvement in storage capacity are illustrated in **Figure 11 a, b**.  
24  
25  
26  
27  
28  
29  
30  
31  
32  
33  
34  
35  
36  
37  
38  
39  
40  
41  
42  
43

44 Lithium intercalation is accomplished by adsorption of lithium ions on the outer crystallite  
45 surface followed by a diffusion of adsorbed lithium ions through the interlayer spaces of  
46 layered 2D materials. Consequently, enhancing intrinsic diffusivity of lithium ions can be  
47 achieved either by introducing interlayer expansion, or by selecting an intercalation host  
48 within an extremely weak interlayer coupling.<sup>[104]</sup> Zhang et al.<sup>[102]</sup> has reported that interlayer  
49 coupling in case of MoS<sub>2</sub> and graphite can partially hinder the massive lithium ions from  
50 being squeezed into the interlayer spaces. A serious problem therefore is volume expansion  
51  
52  
53  
54  
55  
56  
57  
58  
59  
60

1 on lithium intercalation. Alternatively, lithium ions can rapidly diffuse over the layers of ReS<sub>2</sub>  
2  
3 without noticeable volume expansion due to extremely weak vdW interaction between the  
4  
5 layers. The impact of lithium intercalation on volume expansion of ReS<sub>2</sub>, MoS<sub>2</sub> and graphite  
6  
7 is shown schematically in **Figure 11 c**.  
8  
9

10 Li-S batteries (Li-S) are another kind of rechargeable battery and these have the benefits of  
11  
12 high specific capacity (1675 mAh g<sup>-1</sup>) and high specific energy density (2600 Wh kg<sup>-1</sup>) over  
13  
14 LIBs.<sup>[105]</sup> However, Li-S batteries are kinetically sluggish and suffer from poor cycling  
15  
16 efficiency due to dissolution of lithium polysulfides.<sup>[106]</sup> It has shown that ReS<sub>2</sub> can be  
17  
18 exploited as polysulfide immobilizer, and therefore, used to suppress the dissolution of  
19  
20 polysulfides and enhance the cycle stability of the Li-S batteries.<sup>[107]</sup> The effect of ReS<sub>2</sub> in  
21  
22 Li-S batteries has been evaluated by growing vertical nanosheets of ReS<sub>2</sub> (**Figure 12 a**) in  
23  
24 carbon nanofiber (CNF) membrane electrode and using lithium polysulfide (PS) as an active  
25  
26 material. A much improved Coulombic efficiency as well as cycling performance on  
27  
28 PS-ReS<sub>2</sub>@CNF electrode (with ~ 0.063% capacity decay per cycle) was obtained compared  
29  
30 with the PS-CNF electrode (with ~ 0.184 % capacity decay per cycle), as shown in  
31  
32 **Figure 12 b**. Density functional theory (DFT) computation has revealed that there is strong  
33  
34 ionic interactions between negatively charged S atoms of ReS<sub>2</sub> and positively charged Li  
35  
36 cations of Li<sub>x</sub>S<sub>y</sub> molecules (**Figure 12 c**). Moreover, binding polysulfides showed higher  
37  
38 binding energy (2.24 to 2.66 eV) on ReS<sub>2</sub> surfaces than that of carbon (~0.5 to 1 eV).<sup>[108]</sup> As a  
39  
40 result, ReS<sub>2</sub> becomes a more active mediator for adsorbing and trapping polysulfides than  
41  
42 conventional carbon-based surfaces. This leads to alleviation of the dissolution of lithium  
43  
44 polysulfides and improvement in battery performance.  
45  
46  
47  
48  
49  
50  
51  
52  
53

### 54 **6.3. Photocatalytic and electrocatalytic hydrogen evolution**

55 Photocatalysts are semiconductor materials that can absorb solar photon to generate free-  
56  
57 carriers (electrons-holes) to drive the catalytic redox reactions on the surface/terminal sites of  
58  
59  
60

1 a semiconductor.<sup>[109]</sup> Photocatalytic water-splitting, carbon dioxide reduction and pollutant  
2 removals are the hot research topics at present.<sup>[110]</sup> Photocatalysts are the center piece of these  
3 photocatalysis processes for environmental and energy applications.  
4  
5

6  
7  
8 Transition metals dichalcogenide (TMD) are important photocatalyst materials.<sup>[111]</sup> A  
9 selected list of TMD photocatalysts and respective band positions is illustrated in  
10 **Figure 13.** MoS<sub>2</sub> and WS<sub>2</sub> have been extensively studied TMDs in photocatalytic hydrogen  
11 production and pollutant degradation.<sup>[112]</sup> TMDs are layered materials and therefore readily  
12 exfoliated into 2D monolayers. These 2D layered materials exhibit two main advantages: one  
13 is high surface area, and; the other is reduced migration distance for photogenerated electron-  
14 hole pairs. The first advantage provides abundant reaction sites, and; the second reduces the  
15 possibility of electron-hole recombination. This potentially enhances the photocatalytic  
16 performance over the bulk counterpart, and in doing so sparks tremendous interest for  
17 photocatalytic applications.<sup>[113]</sup> However, electronic structure of 2D TMDs is strongly layered  
18 dependent and precise control of the number of layers is rate-determining for optimal catalytic  
19 performance.<sup>[19, 86]</sup> For example, the photocatalytic hydrogen production by MoS<sub>2</sub>  
20 significantly deteriorates when it goes from monolayers to tri-layers.<sup>[114]</sup> The challenges of  
21 layers control is a serious drawback that limits the usage of TMDs in photocatalytic  
22 applications. This is not the case for ReS<sub>2</sub>. ReS<sub>2</sub> has layers independent electronic and  
23 vibrational properties that make it special among reported TMDs.<sup>[20]</sup>  
24  
25  
26  
27  
28  
29  
30  
31  
32  
33  
34  
35  
36  
37  
38  
39  
40  
41  
42  
43  
44  
45  
46

47 Liu et al. have recently explored the potential of photocatalytic water-splitting over ReS<sub>2</sub>  
48 based on *ab initio* calculations.<sup>[115]</sup> In fact this is the only reported research to date on  
49 assessing suitability of ReS<sub>2</sub> as a photocatalyst. For a given semiconductor to qualify as a  
50 water-splitting photocatalyst, two fundamental requirements are simultaneously needed to be  
51 meet: bandgap and band positions.<sup>[116]</sup> ReS<sub>2</sub> has an experimental bandgap of 1.55 eV for  
52 monolayers.<sup>[20]</sup> The theoretical bandgap of ReS<sub>2</sub> varies between 1.89 eV for monolayers to  
53  
54  
55  
56  
57  
58  
59  
60

1 1.76 eV for bulk. For monolayer ReS<sub>2</sub>, the conduction band minimum (CBM) and valence  
2 band maximum (VBM) are located at - 6.15 and - 4.26, eV respectively, relative to vacuum  
3 level.<sup>[115]</sup> Water reduction level is located at -4.44 eV whilst water oxidation level is located  
4 at -5.67 eV relative to vacuum level (consequently, the minimum bandgap required for water  
5 redox reactions is 1.23 eV).<sup>[117]</sup> Compared with water redox level, CBM of ReS<sub>2</sub> is more  
6 negative than water reduction level and VBM is more positive than water oxidation level,  
7 confirming the water-splitting potential of ReS<sub>2</sub>. The positions of CBM and VBM remain  
8 almost unchanged irrespective of layers numbers (*see Figure 14*), suggesting that monolayers  
9 to multilayers ReS<sub>2</sub> is suitable as photocatalyst.<sup>[115]</sup> However, no practical attempt has been  
10 made to demonstrate the photocatalytic activities of ReS<sub>2</sub>.  
11  
12  
13  
14  
15  
16  
17  
18  
19  
20  
21  
22  
23  
24

25 The stability of group VI TMDs depend on the crystal phases of a given material. For  
26 example, 1T phase exhibits superior and more stable hydrogen evolution than 2H phase. This  
27 is because of metallic characteristic of 1T phase and the location of catalytically active sites  
28 on its basal plane.<sup>[118]</sup> However 1T phase is metastable.<sup>[47]</sup> Therefore, 2H phase is the  
29 commonly and widely used phase for group VI TMDs photocatalysts. However, the active  
30 sites of 2H phase are located at the edges that are prone to oxidation, and consequently,  
31 results in vulnerable to instability of the photocatalyst. In addition, high electrical resistance  
32 of 2H phase limits the charge transfer kinetics. This has a parasitic impact on photocatalytic  
33 activity.<sup>[119]</sup> On the other hand, ReS<sub>2</sub> has natural 1T phase and therefore, is thought to be a  
34 highly stable photocatalyst with a high turnover.  
35  
36  
37  
38  
39  
40  
41  
42  
43  
44  
45  
46  
47  
48

49 Hydrogen evolution by electrochemical pathways is another important alternative approach  
50 for clean fuel generation.<sup>[120]</sup> Pt is the oldest and most efficient commercial electrocatalyst for  
51 hydrogen evolution reaction (HER). However, Pt is a rare- earth and a precious noble metal.  
52 Therefore the search for low-cost materials comparable in performance with Pt is ongoing.  
53 TMDs appear as a suitable alternative to Pt catalysts.<sup>[121]</sup> Like other TMDs, ReS<sub>2</sub> has shown  
54  
55  
56  
57  
58  
59  
60  
61  
62  
63  
64  
65

1 good HER performance - better than the more commonly used TMDs.<sup>[107, 122]</sup> Gao et al.<sup>[107]</sup>  
2  
3 has tested HER on CVD grown ReS<sub>2</sub>@Au, and found that it exhibited ~ 200 mV less  
4  
5 overpotential ( $\eta$ ) than bare Au. Further decrease in overpotential ( $\eta < 100$  mV) was achieved  
6  
7 after lithiation using n-butyl lithium treatment (**Figure 15 a**). Lithiation induced some defects  
8  
9 in ReS<sub>2</sub>@Au vertical flakes which were expected to act as active sites. ReS<sub>2</sub> films displayed  
10  
11 high catalytic stability too. For example, after 1000 cycles of operation, just a 15 % decay in  
12  
13 current density was observed. The resultant exchange current density ( $\sim 67.6 \mu\text{A cm}^{-2}$ ),  
14  
15 extrapolated from Tafel plots, was claimed to be significantly greater than those with other  
16  
17 TMDs (**Figure 15 b, c**). In another study carried out by Lu et al., it was shown that HER  
18  
19 could occur at much lower potential on ReS<sub>2</sub> than on glassy carbon and MoS<sub>2</sub>.<sup>[113]</sup> The  
20  
21 reported potentials were -751, - 453 and -336 mV for glassy carbon, MoS<sub>2</sub> and ReS<sub>2</sub>,  
22  
23 respectively (**Figure 15 d**). These results suggest that ReS<sub>2</sub> might actually be an outstanding  
24  
25 electrocatalyst for hydrogen evolution reaction.  
26  
27  
28  
29  
30  
31  
32  
33

## 34 **7. Conclusions and Future Perspective**

35  
36 ReS<sub>2</sub> a least-known transition metal dichalcogenides, has unusual but exciting  
37  
38 physicochemical properties. It has been shown to have potential for a wide range of important  
39  
40 applications in solid state devices including transistors and photodetectors, and catalytic  
41  
42 hydrogen production and lithium ion batteries.  
43  
44

45  
46 ReS<sub>2</sub> is an anisotropic layered 2D material. Anisotropy in both structural and fundamental  
47  
48 properties of ReS<sub>2</sub> could open-up new and perhaps unexpected applications. For example,  
49  
50 ReS<sub>2</sub> exhibits unequivocal electrical, optical, vibrational and magnetic properties -  
51  
52 irrespective of bulk or monolayer - in contrast to widespread conventional TMDs together  
53  
54 with single layers of van der Waals bonded layered materials (e.g. graphene, h-BN,  
55  
56 phosphorene etc.) where isolation of single layer leads to indirect-to direct gap transition,  
57  
58  
59  
60

1 reduction of dielectric constant, increase of exciton binding energies, and high mobility  
2  
3 electrical transport.  
4

5 With optimization of its fundamental properties ReS<sub>2</sub> is expected to be better for known  
6 applications than alternative TMDs. Rather than a standalone ReS<sub>2</sub> however a heterojunction of  
7  
8 ReS<sub>2</sub> with other layered materials is anticipated to be technologically more important. It is  
9  
10 widely known that heterostructure has overwhelming impact in attaining or improving those  
11  
12 functionalities which might not be possible in standalone semiconductor. For example, a  
13  
14 tandem structure of two semiconductors can endure larger overlap in optical absorption of  
15  
16 solar spectrum, and; enhance the charge separation by suppressing recombination or  
17  
18 delocalizing the charge carriers etc. In the light of these benefits of heterostructure, we  
19  
20 anticipate that it is also possible to tune properties, particularly electro-optical properties, of  
21  
22 ReS<sub>2</sub> by combining it with other semiconductors in a form of heterostructure. Demonstrating  
23  
24 heterojunctions with graphene, phosphorene, h-BN and other TMDs will engender wide  
25  
26 interest and likely lead to new and improved functionalities in existing materials. This will  
27  
28 enable the building of new high-performance devices. However, heterostructure of ReS<sub>2</sub> is yet  
29  
30 to be practically realized, but not impossible.  
31  
32  
33  
34  
35  
36  
37  
38

39 Interlayer coupling and stacking are the key factors in determining electronic structure,  
40  
41 bandgap tunability, quantum hall phases, light polarizations, and magnetic properties. It is  
42  
43 known that layers in ReS<sub>2</sub> are randomly stacked and lacked interlayer coupling for which both  
44  
45 bulk and monolayer experience electronic and vibrational decoupling. The reason for  
46  
47 decoupling is claimed to be the in-plane lattice distortion which inhibits orderly fashion layer  
48  
49 stacking and minimizes the interlayer overlap of wavefunctions. In contrast however, it was  
50  
51 demonstrated in other studies that ReS<sub>2</sub> layers are coupled and orderly stacked. Ultra-low  
52  
53 frequency Raman response of atomically thin ReS<sub>2</sub> was reported to show that it exhibited rich  
54  
55 Raman spectra below 50 cm<sup>-1</sup> which was correlated with interlayer shear and breathing modes.  
56  
57  
58  
59  
60



1 Based on the emergence of these interlayer phonons modes, it has been shown that ReS<sub>2</sub>  
2  
3 layers are coupled and orderly stacked.  
4

5 In other studies it was found that there was both anisotropic and isotropic stacking in ReS<sub>2</sub>,  
6  
7 where the anisotropic-stacked layer showed two-shear modes and isotropic-stacked layer  
8  
9 showed one-shear mode. Due to these modes, it was suggested interlayer coupling between  
10  
11 the ReS<sub>2</sub> layers. To resolve the apparent dispute of interlayer coupling, rigorous experimental  
12  
13 approaches are needed.  
14  
15

16  
17 Tuning optical, magnetic and electrical properties by strain engineering remains relatively  
18  
19 unexplored for ReS<sub>2</sub>. Strain engineering is a unique technique for tuning physical properties at  
20  
21 nanoscale for low dimensional material like ReS<sub>2</sub>. Whilst precise control over atomic  
22  
23 composition and structure is more challenging, low dimensional material from mechanical  
24  
25 perspective could withstand a significant amount of strain before fracture, which in turn could  
26  
27 be an ideal way to locally tune the material properties. For example, wrinkle generated local  
28  
29 strain modulates the optical gap, enhance light emission, induces magnetism and alters the  
30  
31 electrical properties.  
32  
33  
34  
35

36  
37 Research needs to be undertaken to understand the charge transport in ReS<sub>2</sub>. Importantly,  
38  
39 there is significant progress in understanding charge transport properties in other TMDs that  
40  
41 can be built on to elucidate charge transport phenomena in ReS<sub>2</sub>. An understanding of drift-  
42  
43 diffusion of charge transport will be needed to determine and improve the mobilities of the  
44  
45 charge carriers, and the coherent controlling of ballistic current. Charge transport, on which  
46  
47 optimization of performance of devices is inevitably related, can be better addressed through  
48  
49 classical (for macro-micro level) and quasi-classical/quantum approaches (for nano-level and  
50  
51 beyond). A critical understanding of the following domains and subdomains is essential for a  
52  
53 clear elucidation of charge transport in ReS<sub>2</sub>. These are the understanding of: (i) carrier  
54  
55 mobility for a nondegenerate electron gas through relaxation time approximation, dependence  
56  
57  
58  
59  
60

1 of scattering on electron energy, momentum relaxation time, and temperature dependence of  
2 mobilities, (ii) doping modulated charge transport, (iii) high-field carrier transport and hot  
3 carrier extraction, (iv) magneto-transport and Hall-Effect, and (v) recombination mechanisms  
4 and charge carrier separation phenomena. Photoelectron spectroscopy (i.e. static and transient  
5 photoluminescence, time resolved transient absorption etc.) and advanced *ab initio*  
6 simulations can be adopted to realize the charge carrier transport dynamics.  
7

8 Although the synthesis of large-area monolayer is possible for ReS<sub>2</sub>, there are hurdles to be  
9 overcome before large-scale use of ReS<sub>2</sub> for device fabrication. These include: (i) the growth  
10 of high quality single crystal ReS<sub>2</sub>, and; (ii) realization of clean interfaces between ReS<sub>2</sub> and  
11 other materials with low contact resistance. To achieve macroscale (chip-scale) ReS<sub>2</sub>,  
12 sophisticated molecular beam epitaxy (MBE) or selective epitaxy routes, need to be  
13 developed. For controlled anisotropic growth, a detailed understanding of how grains are  
14 formed and arranged needs to be made. Little is presently known about grain boundary  
15 structure of ReS<sub>2</sub>.  
16

17 In addition to the optimization of fundamental properties, research effort must also be  
18 directed to enhance the performances of ReS<sub>2</sub> based electronic and optoelectronic devices,  
19 energy storages and catalytical applications. To augment the on/off ratio and sensitivity of  
20 FET and phototransistors it will be crucial to increase the lifetime and mobilities of charge  
21 carriers, enhancing photonic absorption and efficient utilization of the photogenerated charge  
22 carriers. For ReS<sub>2</sub> based FET and phototransistor, no systematic studies have been carried out  
23 demonstrating a deep understanding of these crucial factors.  
24

25 With application of LiBs, ReS<sub>2</sub> showed significant benefits over other TMDs and graphene.  
26 Particularly, in lithium sulfur batteries where TMDs and graphene have been shown to suffer  
27 from dissolution of polysulfides and unwanted volume expansion, ReS<sub>2</sub> was shown to be  
28 resistant to these. However, significant challenges remain in achieving high specific energy  
29  
30  
31  
32  
33

(energy/weight) and energy density (energy/volume). Research ought to focus on the maintenance of stable structure of electrodes, full utilization of active material, and; adequate cycle life with improved system efficiency. This will necessitate exploration of new electrochemistry. Beside LiB and LiS batteries, the suitability of ReS<sub>2</sub> could be explored for other types of rechargeable batteries, such as Li-O<sub>2</sub>, Zn-air etc.

Based on current theoretical knowledge, ReS<sub>2</sub> could be a new material for photocatalytic applications due to its visible light absorption capabilities and suitable band positions for redox reactions. However, experimental demonstration of it as a photocatalyst has not been reported. Additionally, electrocatalytic hydrogen evolution reaction (HER) on ReS<sub>2</sub> has shed light on its possible future use as an electrocatalyst for oxygen evolution reaction (OER) and oxygen reduction reaction (ORR). Apart from solar-to-chemical energy conversion, ReS<sub>2</sub> can also be employed to fabricate solar cells for harvesting solar energy to produce electrical current. 2D ReS<sub>2</sub> also has potential for strain sensors, stretchable electrodes, artificial muscle actuators and piezoelectric applications for example.

ReS<sub>2</sub> is a versatile material but least-explored among TMDs. Investigation of fundamental properties of ReS<sub>2</sub> has been mostly accomplished through simulations. It is clear more research is needed in experimental studies.

Lastly, Re is not earth-abundant. It is relatively expensive. Synthesis of ReS<sub>2</sub> is cumbersome. Despite its desirable fundamental properties, its techno-economic feasibility will depend on development of scalable and practical syntheses.

## Acknowledgements

This work was financially supported by the Australian Research Council (ARC) through the Discovery Project program (DP130104459, DP140104062 and DP160104866).

Received: ((will be filled in by the editorial staff))

Revised: ((will be filled in by the editorial staff))

Published online: ((will be filled in by the editorial staff))

## References

- 1  
2  
3 [1] K. S. Novoselov, A. K. Geim, S. V. Morozov, D. Jiang, Y. Zhang, S. V. Dubonos, I. V.  
4  
5 Grigorieva, A. A. Firsov, *Science* **2004**, *306*, 666.  
6  
7  
8 [2] A. K. Geim, K. S. Novoselov, *Nat. Mater.* **2007**, *6*, 183.  
9  
10 [3] F. Xia, H. Wang, D. Xiao, M. Dubey, A. Ramasubramaniam, *Nat. Photon.* **2014**, *8*,  
11  
12 899.  
13  
14 [4] a) A. K. Geim, *Science* 2009, *324*, 1530; A. K. Geim, I. V. Grigorieva, *Nature* **2013**,  
15  
16 *499*, 419; b) P. Miro, M. Audiffred, T. Heine, *Chem. Soc. Rev.* **2014**, *43*, 6537.  
17  
18 [5] K. S. Novoselov, D. Jiang, F. Schedin, T. J. Booth, V. V. Khotkevich, S. V. Morozov,  
19  
20 A. K. Geim, *Proc. Nat. Acad. Sci. U. S. A.* **2005**, *102*, 10451.  
21  
22 [6] a) K. Wu, E. Torun, H. Sahin, B. Chen, X. Fan, A. Pant, D. Parsons Wright, T. Aoki, F.  
23  
24 M. Peeters, E. Soignard, S. Tongay, *Nat. Commun.* **2016**, *7*, 12952; b) J. Dai, X. C. Zeng,  
25  
26 *Angew. Chem. Int. Ed.* **2015**, *54*, 7572; c) J. O. Island, R. Biele, M. Barawi, J. M.  
27  
28 Clamagirand, J. R. Ares, C. Sanchez, H. S. van der Zant, I. J. Ferrer, R. D'Agosta, A.  
29  
30 Castellanos-Gomez, *Sci. Rep.* **2016**, *6*, 22214.  
31  
32 [7] J. O. Island, M. Barawi, R. Biele, A. Almazan, J. M. Clamagirand, J. R. Ares, C.  
33  
34 Sanchez, H. S. van der Zant, J. V. Alvarez, R. D'Agosta, I. J. Ferrer, A. Castellanos-Gomez,  
35  
36 *Adv. Mater.* **2015**, *27*, 2595.  
37  
38 [8] A. Pant, E. Torun, B. Chen, S. Bhat, X. Fan, K. Wu, D. P. Wright, F. M. Peeters, E.  
39  
40 Soignard, H. Sahin, S. Tongay, *Nanoscale* **2016**, *8*, 16259.  
41  
42 [9] a) L. Tao, E. Cinquanta, D. Chiappe, C. Grazianetti, M. Fanciulli, M. Dubey, A. Molle,  
43  
44 D. Akinwande, *Nat. Nanotechnol.* **2015**, *10*, 227; b) S. Balendhran, S. Walia, H. Nili, S.  
45  
46 Sriram, M. Bhaskaran, *Small* **2015**, *11*, 640; c) F. Xia, H. Wang, Y. Jia, *Nat. Commun.* **2014**,  
47  
48 *5*, 4458; d) X. Ling, H. Wang, S. Huang, F. Xia, M. S. Dresselhaus, *Proc. Nat. Acad. Sci. U. S.*  
49  
50 *A.* **2015**, *112*, 4523.  
51  
52  
53  
54  
55  
56  
57  
58  
59  
60  
61  
62  
63  
64  
65

- 1 [10] M. Z. Rahman, C. W. Kwong, K. Davey, S. Z. Qiao, *Energy Environ. Sci.* **2016**, *9*,  
2 709.  
3  
4  
5 [11] H. Tian, M. L. Chin, S. Najmaei, Q. Guo, F. Xia, H. Wang, M. Dubey, *Nano Res.*  
6 **2016**, *9*, 1543.  
7  
8  
9 [12] Q. H. Wang, K. Kalantar-Zadeh, A. Kis, J. N. Coleman, M. S. Strano, *Nat.*  
10 *Nanotechnol.* **2012**, *7*, 699.  
11  
12  
13 [13] Y.-C. Lin, H.-P. Komsa, C.-H. Yeh, T. Björkman, Z.-Y. Liang, C.-H. Ho, Y.-S. Huang,  
14 P.-W. Chiu, A. V. Krasheninnikov, K. Suenaga, *ACS Nano* **2015**, *9*, 11249.  
15  
16  
17 [14] E. Gibney, *Nature* **2015**, *522*, 274.  
18  
19  
20 [15] J. A. Wilson, A. D. Yoffe, *Adv. Phys.* **1969**, *18*, 193.  
21  
22  
23 [16] L. Hart, S. Dale, S. Hoye, J. L. Webb, D. Wolverson, *Nano Lett.* **2016**, *16*, 1381.  
24  
25  
26 [17] D. Wolverson, L. S. Hart, *Nanoscale Res. Lett.* **2016**, *11*, 1.  
27  
28  
29 [18] S. Tongay, J. Zhou, C. Ataca, K. Lo, T. S. Matthews, J. Li, J. C. Grossman, J. Wu,  
30 *Nano Lett.* **2012**, *12*, 5576.  
31  
32  
33 [19] W. Jin, P.-C. Yeh, N. Zaki, D. Zhang, J. T. Sadowski, A. Al-Mahboob, A. M. van der  
34 Zande, D. A. Chenet, J. I. Dadap, I. P. Herman, P. Sutter, J. Hone, R. M. Osgood, *Phys. Rev.*  
35 *Lett.* **2013**, *111*, 106801.  
36  
37  
38 [20] S. Tongay, H. Sahin, C. Ko, A. Luce, W. Fan, K. Liu, J. Zhou, Y. S. Huang, C. H. Ho,  
39 J. Yan, D. F. Ogletree, S. Aloni, J. Ji, S. Li, J. Li, F. M. Peeters, J. Wu, *Nat. Commun.* **2014**, *5*,  
40 3252.  
41  
42  
43 [21] D. A. Chenet, O. B. Aslan, P. Y. Huang, C. Fan, A. M. van der Zande, T. F. Heinz, J.  
44 C. Hone, *Nano Lett.* **2015**, *15*, 5667.  
45  
46  
47 [22] S. Ge, C. Li, Z. Zhang, C. Zhang, Y. Zhang, J. Qiu, Q. Wang, J. Liu, S. Jia, J. Feng, D.  
48 Sun, *Nano Lett.* **2015**, *15*, 4650.  
49  
50  
51  
52  
53  
54  
55  
56  
57  
58  
59  
60  
61  
62  
63  
64  
65

- 1 [23] B. Jariwala, D. Voiry, A. Jindal, B. A. Chalke, R. Bapat, A. Thamizhavel, M.  
2 Chhowalla, M. Deshmukh, A. Bhattacharya, *Chem. Mater.* **2016**, 28, 3352.  
3  
4 [24] H. H. Murray, S. P. Kelty, R. R. Chianelli, C. S. Day, *Inorg. Chem.* **1994**, 33, 4418.  
5  
6 [25] D. Wolverson, L. S. Hart, *Nanoscale Res. Lett.* **2016**, 11, 250.  
7  
8 [26] E. Liu, Y. Fu, Y. Wang, Y. Feng, H. Liu, X. Wan, W. Zhou, B. Wang, L. Shao, C. H.  
9 Ho, Y. S. Huang, Z. Cao, L. Wang, A. Li, J. Zeng, F. Song, X. Wang, Y. Shi, H. Yuan, H. Y.  
10 Hwang, Y. Cui, F. Miao, D. Xing, *Nat. Commun.* **2015**, 6, 6991.  
11  
12 [27] E. Liu, M. Long, J. Zeng, W. Luo, Y. Wang, Y. Pan, W. Zhou, B. Wang, W. Hu, Z. Ni,  
13 Y. You, X. Zhang, S. Qin, Y. Shi, K. Watanabe, T. Taniguchi, H. Yuan, H. Y. Hwang, Y. Cui,  
14 F. Miao, D. Xing, *Adv. Funct. Mater.* **2016**, 26, 1938.  
15  
16 [28] J. Lu, H. Liu, E. S. Tok, C. H. Sow, *Chem. Soc. Rev.* **2016**, 45, 2494;  
17  
18 [29] a) B. Peng, P. K. Ang, K. P. Loh, *Nano Today* **2015**, 10, 128; b) C. Xie, C. Mak, X.  
19 Tao, F. Yan, *Funct. Mater.* **2016**, Doi: 10.1002/adfm.201603886.  
20  
21 [30] I. T. W. Noddack, and O. Berg, *Naturwissenschaften* **1925**, 13, 567.  
22  
23 [31] E. Scerri, *Nat. Chem.* **2010**, 2, 598.  
24  
25 [32] G. Rouschias, *Chem. Revi.* **1974**, 74, 531.  
26  
27 [33] H. H. Murray, L. Wei, S. E. Sherman, M. A. Greaney, K. A. Eriksen, B. Carstensen, T.  
28 R. Halbert, E. I. Stiefel, *Inorg. Chem.* **1995**, 34, 841.  
29  
30 [34] J. T. Alexander V. Kolobov, *Two dimensional Transition Metal Dichalcogenides*,  
31 Springer **2016**.  
32  
33 [35] X. Zhang, Q. Li, *J. Appl. Phys.* **2015**, 118, 064306.  
34  
35 [36] S. P. Kelty, A. F. Ruppert, R. R. Chianelli, J. Ren, M. H. Whangbo, *J. Am. Chem. Soc.*  
36 **1994**, 116, 7857.  
37  
38  
39  
40  
41  
42  
43  
44  
45  
46  
47  
48  
49  
50  
51  
52  
53  
54  
55  
56  
57  
58  
59  
60  
61  
62  
63  
64  
65

- [37] K. Keyshar, Y. Gong, G. Ye, G. Brunetto, W. Zhou, D. P. Cole, K. Hackenberg, Y. He, L. Machado, M. Kabbani, A. H. Hart, B. Li, D. S. Galvao, A. George, R. Vajtai, C. S. Tiwary, P. M. Ajayan, *Adv. Mater.* **2015**, 27, 4640.
- [38] F. Cui, C. Wang, X. Li, G. Wang, K. Liu, Z. Yang, Q. Feng, X. Liang, Z. Zhang, S. Liu, Z. Lei, Z. Liu, H. Xu, J. Zhang, *Adv. Mater.* **2016**, 28, 5019–5024.
- [39] X. He, F. Liu, P. Hu, W. Fu, X. Wang, Q. Zeng, W. Zhao, Z. Liu, *Small* **2015**, 11, 5423.
- [40] T. Fujita, Y. Ito, Y. Tan, H. Yamaguchi, D. Hojo, A. Hirata, D. Voiry, M. Chhowalla, M. Chen, *Nanoscale* **2014**, 6, 12458.
- [41] N. Al-Dulaimi, E. A. Lewis, D. J. Lewis, S. K. Howell, S. J. Haigh, P. O'Brien, *Chem Commun* **2016**, 52, 7878.
- [42] M. Hafeez, L. Gan, H. Li, Y. Ma, T. Zhai, *Adv. Funct. Mater.* **2016**, 26, 4551- 4560.
- [43] J. Kang, V. K. Sangwan, J. D. Wood, X. Liu, I. Balla, D. Lam, M. C. Hersam, *Nano Lett.* **2016**, DOI: 10.1021/acs.nanolett.6b03584.
- [44] a) B. L. Wheeler, J. K. Leland, A. J. Bard, *J. Electrochem. Soc.* **1986**, 133, 358; b) G. Leicht, H. Berger, F. Levy, *Solid State Commun.* **1987**, 61, 531.
- [45] X. Li, F. Cui, Q. Feng, G. Wang, X. Xu, J. Wu, N. Mao, X. Liang, Z. Zhang, J. Zhang, H. Xu, *Nanoscale* **2016**, DOI: 10.1039/c6nr07233j.
- [46] M. Chhowalla, H. S. Shin, G. Eda, L. J. Li, K. P. Loh, H. Zhang, *Nat. Chem.* **2013**, 5, 263.
- [47] X. Lu, X. Luo, J. Zhang, S. Y. Quek, Q. Xiong, *Nano Res.* 2016, DOI: 10.1007/s12274-016-1224-5.
- [48] a) R. A. Gordon, D. Yang, E. D. Crozier, D. T. Jiang, R. F. Frindt, *Phys. Rev. B* **2002**, 65, 125407; b) S. W. Han, H. Kwon, S. K. Kim, S. Ryu, W. S. Yun, D. H. Kim, J. H. Hwang,

- 1 J. S. Kang, J. Baik, H. J. Shin, S. C. Hong, *Phys. Rev. B* **2011**, *84*, 045409; c) J. K. Ellis, M. J.  
2  
3 Lucero, G. E. Scuseria, *Appl. Phys. Lett.* **2011**, *99*, 261908.  
4  
5 [49] K. F. Mak, C. Lee, J. Hone, J. Shan, T. F. Heinz, *Phys. Rev. Lett.* **2010**, *105*, 136805.  
6  
7 [50] S. Horzum, D. Çakır, J. Suh, S. Tongay, Y. S. Huang, C. H. Ho, J. Wu, H. Sahin, F. M.  
8  
9 Peeters, *Phys. Rev. B* **2014**, *89*, 155433.  
10  
11 [51] C. H. Ho, Y. S. Huang, K. K. Tiong, P. C. Liao, *Phys. Rev. B* **1998**, *58*, 16130.  
12  
13 [52] K. Friemelt, S. Akari, M. C. Lux-Steiner, T. Schill, E. Bucher, K. Dransfeld, *Ann.*  
14  
15 *Phys.* **1992**, *504*, 248.  
16  
17 [53] X. F. Qiao, J. B. Wu, L. Zhou, J. Qiao, W. Shi, T. Chen, X. Zhang, J. Zhang, W. Ji, P.  
18  
19 H. Tan, *Nanoscale* **2016**, *8*, 8324.  
20  
21 [54] R. He, J. A. Yan, Z. Yin, Z. Ye, G. Ye, J. Cheng, J. Li, C. H. Lui, *Nano Lett.* **2016**, *16*,  
22  
23 1404.  
24  
25 [55] E. Lorchat, G. Froehlicher, S. Berciaud, *ACS Nano* **2016**, *10*, 2752.  
26  
27 [56] Q. Zhang, W. Wang, X. Kong, R. G. Mendes, L. Fang, Y. Xue, Y. Xiao, M. H.  
28  
29 Rummeli, S. Chen, L. Fu, *J. Am. Chem. Soc.* **2016**, *138*, 11101.  
30  
31 [57] M. Brorson, T. W. Hansen, C. J. H. Jacobsen, *J. Am. Chem. Soc.* **2002**, *124*, 11582.  
32  
33 [58] K. Wu, B. Chen, S. Yang, G. Wang, W. Kong, H. Cai, T. Aoki, E. Soignard, X. Marie,  
34  
35 A. Yano, A. Suslu, B. Urbaszek, S. Tongay, *Nano Lett.* **2016**, *16*, 5888-5894.  
36  
37 [59] a) W. Guo, B. Wu, Y. Li, L. Wang, J. Chen, B. Chen, Z. Zhang, L. Peng, S. Wang, Y.  
38  
39 Liu, *ACS Nano* **2015**, *9*, 5792; b) P. Y. Huang, C. S. Ruiz-Vargas, A. M. van der Zande, W. S.  
40  
41 Whitney, M. P. Levendorf, J. W. Kevek, S. Garg, J. S. Alden, C. J. Hustedt, Y. Zhu, J. Park, P.  
42  
43 L. McEuen, D. A. Muller, *Nature* **2011**, *469*, 389.  
44  
45 [60] a) S. Najmaei, Z. Liu, W. Zhou, X. Zou, G. Shi, S. Lei, B. I. Yakobson, J.-C. Idrobo, P.  
46  
47 M. Ajayan, J. Lou, *Nat. Mater.* **2013**, *12*, 754; b) Y. Liu, X. Zou, B. I. Yakobson, *ACS Nano*  
48  
49  
50  
51  
52  
53  
54  
55  
56  
57  
58  
59  
60  
61  
62  
63  
64  
65



- 1 **2012**, 6, 7053; c) A. L. Gibb, N. Alem, J.-H. Chen, K. J. Erickson, J. Ciston, A. Gautam, M.  
2  
3 Linck, A. Zettl, *J. Am. Chem. Soc.* **2013**, 135, 6758.  
4  
5 [61] D. Wolverson, S. Crampin, A. S. Kazemi, A. Ilie, S. J. Bending, *ACS Nano* **2014**, 8,  
6  
7 11154.  
8  
9  
10 [62] Y. Feng, W. Zhou, Y. Wang, J. Zhou, E. Liu, Y. Fu, Z. Ni, X. Wu, H. Yuan, F. Miao,  
11  
12 B. Wang, X. Wan, D. Xing, *Phys. Rev. B* **2015**, 92, 054110.  
13  
14  
15 [63] K. K. Tiong, C. H. Ho, Y. S. Huang, *Solid State Commun.* **1999**, 111, 635.  
16  
17  
18 [64] S. Yang, J. Kang, Q. Yue, J. M. D. Coey, C. Jiang, *Adv. Mater. Interfaces* **2016**, 3,  
19  
20 1500707.  
21  
22  
23 [65] K. Friemelt, L. Kulikova, L. Kulyuk, A. Siminel, E. Arushanov, C. Kloc, E. Bucher, *J.*  
24  
25 *Appl. Phys.* **1996**, 79, 9268.  
26  
27  
28 [66] a) C. Lee, H. Yan, L. E. Brus, T. F. Heinz, J. Hone, S. Ryu, *ACS Nano* **2010**, 4, 2695;  
29  
30 b) H. Sahin, S. Tongay, S. Horzum, W. Fan, J. Zhou, J. Li, J. Wu, F. M. Peeters, *Phys. Rev. B*  
31  
32 **2013**, 87, 165409; c) A. Berkdemir, H. R. Gutiérrez, A. R. Botello-Méndez, N. Perea-López,  
33  
34 A. L. Elías, C.-I. Chia, B. Wang, V. H. Crespi, F. López-Urías, J.-C. Charlier, H. Terrones, M.  
35  
36 Terrones, *Sci. Reports* **2013**, 3, 1755; d) P. Nagler, G. Plechinger, C. Schüller, T. Korn, *Phys.*  
37  
38 *Status Solidi (RRL)* **2016**, 10, 185; e) J. Lin, L. Liang, X. Ling, S. Zhang, N. Mao, N. Zhang,  
39  
40 B. G. Sumpter, V. Meunier, L. Tong, J. Zhang, *J. Am. Chem. Soc.* **2015**, 137, 15511;  
41  
42  
43 [67] S. Yu, H. Zhu, K. Eshun, C. Shi, M. Zeng, Q. Li, *Appl. Phys. Lett.* **2016**, 108, 191901.  
44  
45  
46 [68] Q. Cui, H. Zhao, *ACS Nano* **2015**, 9, 3935.  
47  
48  
49 [69] N. R. Pradhan, A. McCreary, D. Rhodes, Z. Lu, S. Feng, E. Manousakis, D. Smirnov,  
50  
51 R. Namburu, M. Dubey, A. R. Walker, H. Terrones, M. Terrones, V. Dobrosavljevic, L.  
52  
53 Balicas, *Nano Lett.* **2015**, 15, 8377.  
54  
55  
56 [70] O. B. Aslan, D. A. Chenet, A. M. van der Zande, J. C. Hone, T. F. Heinz, *ACS Photon.*  
57  
58 **2016**, 3, 96.  
59  
60  
61  
62  
63  
64  
65

- [71] K. Friemelt, M. C. Lux-Steiner, E. Bucher, *J. Appl. Phys.* **1993**, *74*, 5266.
- [72] Q. Cui, J. He, M. Z. Bellus, M. Mirzokarimov, T. Hofmann, H. Y. Chiu, M. Antonik, D. He, Y. Wang, H. Zhao, *Small* **2015**, *11*, 5565.
- [73] H.-X. Zhong, S. Gao, J.-J. Shi, L. Yang, *Phys. Rev. B* **2015**, *92*, 115438.
- [74] D. Cakir, H. Sahin, F. M. Peeters, *Phys. Chem. Chem. Phys.* **2014**, *16*, 16771.
- [75] G. C. Loh, R. Pandey, *Phys. Chem. Chem. Phys.* **2015**, *17*, 18843.
- [76] a) D. O. Dumcenco, Y. S. Huang, C. H. Liang, K. K. Tiong, *J. Appl. Phys.* **2007**, *102*, 083523; b) C. H. Ho, P. C. Liao, Y. S. Huang, K. K. Tiong, *Phys. Rev. B* **1997**, *55*, 15608.
- [77] C. H. Ho, P. C. Yen, Y. S. Huang, K. K. Tiong, *Phys. Rev. B* **2002**, *66*, 15608-15613.
- [78] T. P. Kaloni, G. Schreckenbach, M. S. Freund, *J. Phys. Chem. C* **2014**, *118*, 23361; T. P. Kaloni, *J. Phys. Chem. C* **2014**, *118*, 25200.
- [79] a) G. Henkelman, A. Arnaldsson, H. Jónsson, *Comput. Mater. Sci.* **2006**, *36*, 354; b) E. Sanville, S. D. Kenny, R. Smith, G. Henkelman, *J. Comput. Chem.* **2007**, *28*, 899.
- [80] M. Wu, C. Cao, J. Z. Jiang, *Nanotechnology* **2010**, *21*, 505202.
- [81] a) J. He, K. Wu, R. Sa, Q. Li, Y. Wei, *Appl. Phys. Lett.* **2010**, *96*, 082504; b) J. Chang, S. Larentis, E. Tutuc, L. F. Register, S. K. Banerjee, *Appl. Phys. Lett.* **2014**, *104*, 141603; c) P. Rastogi, S. Kumar, S. Bhowmick, A. Agarwal, Y. S. Chauhan, *J. Phys. Chem. C* **2014**, *118*, 30309; d) D. Gao, S. Shi, K. Tao, B. Xia, D. Xue, *Nanoscale* **2015**, *7*, 4211.
- [82] a) L. Shen, R. Q. Wu, H. Pan, G. W. Peng, M. Yang, Z. D. Sha, Y. P. Feng, *Phys. Rev. B* **2008**, *78*, 073306; b) O. V. Yazyev, L. Helm, *Phys. Rev. B* **2007**, *75*, 125408.
- [83] M. Segal, *Nature* **2012**, *483*, S43; K. Bourzac, *Nature* **2012**, *483*, S34; F. Schwierz, *Proc. IEEE* **2013**, *101*, 1567.
- [84] F. Schwierz, J. Pezoldt, R. Granzner, *Nanoscale* **2015**, *7*, 8261.
- [85] A. Splendiani, L. Sun, Y. Zhang, T. Li, J. Kim, C.-Y. Chim, G. Galli, F. Wang, *Nano Lett.* **2010**, *10*, 1271.

- 1 [86] W. Zhao, R. M. Ribeiro, M. Toh, A. Carvalho, C. Kloc, A. H. Castro Neto, G. Eda,  
2  
3 *Nano Lett.* **2013**, *13*, 5627.  
4
- 5 [87] C. M. Corbet, C. McClellan, A. Rai, S. S. Sonde, E. Tutuc, S. K. Banerjee, *ACS Nano*  
6  
7 **2015**, *9*, 363.  
8
- 9 [88] K. Xu, H. X. Deng, Z. Wang, Y. Huang, F. Wang, S. S. Li, J. W. Luo, J. He,  
10  
11 *Nanoscale* **2015**, *7*, 15757.  
12
- 13 [89] E. Zhang, Y. Jin, X. Yuan, W. Wang, C. Zhang, L. Tang, S. Liu, P. Zhou, W. Hu, F.  
14  
15 Xiu, *Adv. Funct. Mater.* **2015**, *25*, 4076.  
16
- 17 [90] F. Liu, S. Zheng, X. He, A. Chaturvedi, J. He, W. L. Chow, T. R. Mion, X. Wang, J.  
18  
19 Zhou, Q. Fu, H. J. Fan, B. K. Tay, L. Song, R.-H. He, C. Kloc, P. M. Ajayan, Z. Liu, *Adv.*  
20  
21 *Funct. Mater.* **2016**, *26*, 1169.  
22
- 23 [91] J. Shim, A. Oh, D. H. Kang, S. Oh, S. K. Jang, J. Jeon, M. H. Jeon, M. Kim, C. Choi, J.  
24  
25 Lee, S. Lee, G. Y. Yeom, Y. J. Song, J. H. Park, *Adv. Mater.* **2016**, *28*, 6985-6992.  
26
- 27 [92] C. M. Corbet, S. S. Sonde, E. Tutuc, S. K. Banerjee, *Appl. Phys. Lett.* **2016**, *108*,  
28  
29 162104.  
30
- 31 [93] M. Najmzadeh, C. Ko, K. Wu, S. Tongay, J. Wu, *Appl. Phys. Express* **2016**, *9*, 055201.  
32
- 33 [94] I. Ferain, C. A. Colinge, J.-P. Colinge, *Nature* **2011**, *479*, 310.  
34
- 35 [95] a) R. R. Nair, W. Ren, R. Jalil, I. Riaz, V. G. Kravets, L. Britnell, P. Blake, F. Schedin,  
36  
37 A. S. Mayorov, S. Yuan, M. I. Katsnelson, H.-M. Cheng, W. Strupinski, L. G. Bulusheva, A.  
38  
39 V. Okotrub, I. V. Grigorieva, A. N. Grigorenko, K. S. Novoselov, A. K. Geim, *Small* **2010**, *6*,  
40  
41 2877; b) L. Li, Y. Yu, G. J. Ye, Q. Ge, X. Ou, H. Wu, D. Feng, X. H. Chen, Y. Zhang, *Nat.*  
42  
43 *Nanotechnol.* **2014**, *9*, 372; c) H. Liu, A. T. Neal, Z. Zhu, Z. Luo, X. Xu, D. Tománek, P. D.  
44  
45 Ye, *ACS Nano* **2014**, *8*, 4033.  
46
- 47 [96] RadisavljevicB, RadenovicA, BrivioJ, GiacomettiV, KisA, *Nat. Nanotechnol.* **2011**, *6*,  
48  
49 147.  
50  
51  
52  
53  
54  
55  
56  
57  
58  
59  
60  
61  
62  
63  
64  
65

- 1 [97] R. Sordan, F. Traversi, V. Russo, *Appl. Phys. Lett.* **2009**, *94*, 073305.  
2  
3 [98] a) R. Cheng, S. Jiang, Y. Chen, Y. Liu, N. Weiss, H.-C. Cheng, H. Wu, Y. Huang, X.  
4 Duan, *Nat. Commun.* **2014**, *5*, 5143 ; b) H. Wang, L. Yu, Y.-H. Lee, Y. Shi, A. Hsu, M. L.  
5 Chin, L.-J. Li, M. Dubey, J. Kong, T. Palacios, *Nano Lett.* **2012**, *12*, 4674; c) S.-L. Li, H.  
6 Miyazaki, A. Kumatani, A. Kanda, K. Tsukagoshi, *Nano Lett.* **2010**, *10*, 2357.  
7  
8 [99] a) X. Cao, Y. Shi, W. Shi, X. Rui, Q. Yan, J. Kong, H. Zhang, *Small* **2013**, *9*, 3433; b)  
9 W. Gu, A. Magasinski, B. Zdyrko, G. Yushin, *Adv. Energy Mater.* **2015**, *5*, 1570019; c) Y.-J.  
10 Han, J. Kim, J.-S. Yeo, J. C. An, I.-P. Hong, K. Nakabayashi, J. Miyawaki, J.-D. Jung, S.-H.  
11 Yoon, *Carbon* **2015**, *94*, 432.  
12  
13 [100] J. B. Goodenough, Y. Kim, *Chem. Mater.* **2010**, *22*, 587.  
14  
15 [101] a) J. Xiao, D. Choi, L. Cosimbescu, P. Koech, J. Liu, J. P. Lemmon, *Chem. Mater.*  
16 2010, *22*, 4522; b) H. Shi, J. Barker, M. Y. Saïdi, R. Koksang, *J. Electrochem. Soc.* **1996**,  
17 *143*, 3466.  
18  
19 [102] Q. Zhang, S. Tan, R. G. Mendes, Z. Sun, Y. Chen, X. Kong, Y. Xue, M. H. Rummeli,  
20 X. Wu, S. Chen, L. Fu, *Adv. Mater.* **2016**, *28*, 2616.  
21  
22 [103] a) C. M. Fang, G. A. Wiegers, C. Haas, R. A. d. Groot, *J. Phys.: Condens. Matter*  
23 **1997**, *9*, 4411; b) J. He, C. Zhang, H. Du, S. Zhang, P. Hu, Z. Zhang, Y. Ma, C. Huang, G.  
24 Cui, *Electrochim. Acta* **2015**, *178*, 476.  
25  
26 [104] Y. Liang, H. D. Yoo, Y. Li, J. Shuai, H. A. Calderon, F. C. Robles Hernandez, L. C.  
27 Grabow, Y. Yao, *Nano Lett.* **2015**, *15*, 2194.  
28  
29 [105] a) P. G. Bruce, S. A. Freunberger, L. J. Hardwick, J. M. Tarascon, *Nat. Mater.* **2012**,  
30 *11*, 19; b) Y. X. Yin, S. Xin, Y. G. Guo, L. J. Wan, *Angew. Chem. Int. Ed.* **2013**, *52*, 13186.  
31  
32 [106] a) Q. Zhang, Y. Wang, Z. W. Seh, Z. Fu, R. Zhang, Y. Cui, *Nano Lett.* **2015**, *15*, 3780;  
33 b) Z. Yuan, H.-J. Peng, T.-Z. Hou, J.-Q. Huang, C.-M. Chen, D.-W. Wang, X.-B. Cheng, F.  
34  
35  
36  
37  
38  
39  
40  
41  
42  
43  
44  
45  
46  
47  
48  
49  
50  
51  
52  
53  
54  
55  
56  
57  
58  
59  
60  
61  
62  
63  
64  
65

1 Wei, Q. Zhang, *Nano Lett.* **2016**, *16*, 519, c) A. Manthiram, Y. Fu, Y.-S. Su, *Acc. Chem.*  
2  
3 *Research* **2013**, *46*, 1125.

4  
5 [107] J. Gao, L. Li, J. Tan, H. Sun, B. Li, J. C. Idrobo, C. V. Singh, T. M. Lu, N. Koratkar,  
6  
7 *Nano Lett.* **2016**, *16*, 3780.

8  
9  
10 [108] Y. Qiu, W. Li, W. Zhao, G. Li, Y. Hou, M. Liu, L. Zhou, F. Ye, H. Li, Z. Wei, S.  
11  
12 Yang, W. Duan, Y. Ye, J. Guo, Y. Zhang, *Nano Lett.* **2014**, *14*, 4821.

13  
14 [109] a) M. Grätzel, *Philos. Trans. Royal Soci. London A: Math., Phys. and Eng. Sci.* **2007**,  
15  
16 *365*, 993; b) M. Gratzel, *Nature* **2001**, *414*, 338; c) M. G. Walter, E. L. Warren, J. R. McKone,  
17  
18 S. W. Boettcher, Q. Mi, E. A. Santori, N. S. Lewis, *Chem. Rev.* **2010**, *110*, 6446; d) K. Maeda,  
19  
20 K. Teramura, D. Lu, T. Takata, N. Saito, Y. Inoue, K. Domen, *Nature* **2006**, *440*, 295; e) M. Z.  
21  
22 Rahman, J. Zhang, Y. Tang, K. Davey, S.-Z. Qiao, *Mater. Chem. Front.* **2017**, DOI:  
23  
24 10.1039/C6QM00241B.

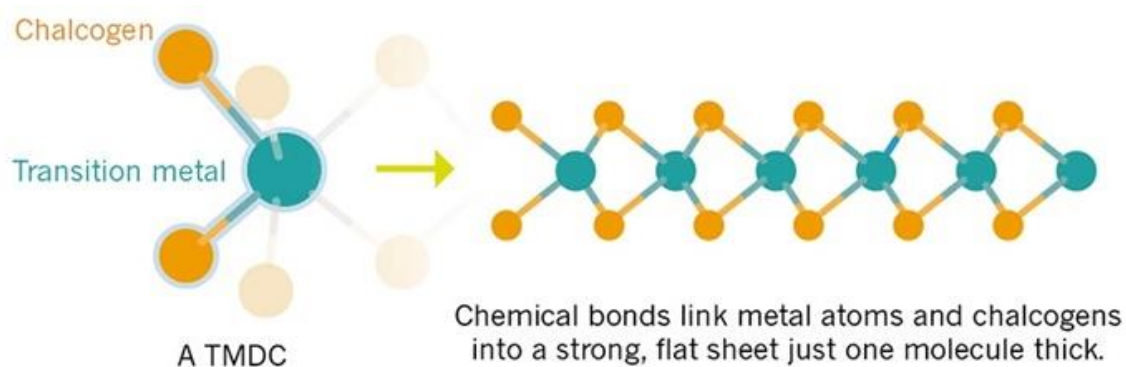
25  
26 [110] a) H. Kisch, *Angew. Chem. Int. Ed.* **2013**, *52*, 812; b) M. Z. Rahman, J. Ran, Y. Tang,  
27  
28 M. Jaroniec, S. Z. Qiao, *J. Mater. Chem. A* **2016**, *4*, 2445; c) X. Meng, L. Liu, S. Ouyang, H.  
29  
30 Xu, D. Wang, N. Zhao, J. Ye, *Adv. Mater.* **2016**, *28*, 6781-6803 ; d) M. N. Chong, B. Jin, C.  
31  
32 W. K. Chow, C. Saint, *Water Res.* **2010**, *44*, 2997; e) E. V. Kondratenko, G. Mul, J.  
33  
34 Baltrusaitis, G. O. Larrazabal, J. Perez-Ramirez, *Energy Environ. Sci.* **2013**, *6*, 3112; f) D. D.  
35  
36 Zhu, J. L. Liu, S. Z. Qiao, *Adv. Mater.* **2016**, *28*, 3423.

37  
38 [111] a) X. Huang, Z. Zeng, H. Zhang, *Chem. Soc. Rev.* **2013**, *42*, 1934; b) H. L. Zhuang, R.  
39  
40 G. Hennig, *J. Phys. Chem. C* **2013**, *117*, 20440.

41  
42 [112] a) H. Jiang, *J. Phys. Chem. C* **2012**, *116*, 7664; b) W. Zhou, Z. Yin, Y. Du, X. Huang,  
43  
44 Z. Zeng, Z. Fan, H. Liu, J. Wang, H. Zhang, *Small* **2013**, *9*, 140; c) H. L. Zhuang, R. G.  
45  
46 Hennig, *Chem. Mater.* **2013**, *25*, 3232.  
47  
48  
49  
50  
51  
52  
53  
54  
55  
56  
57  
58  
59  
60  
61  
62  
63  
64  
65

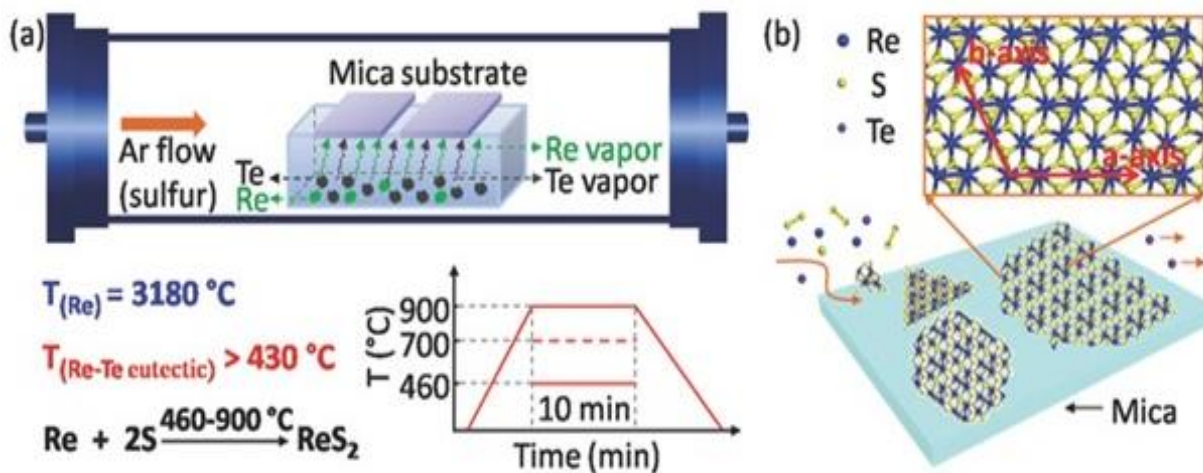
- 1 [113] a) A. K. Singh, K. Mathew, H. L. Zhuang, R. G. Hennig, *J. Phys. Chem. Lett.* **2015**, *6*,  
2 1087; b) J. Zhang, Y. Chen, X. Wang, *Energy Environ. Sci.* **2015**, *8*, 3092; c) B. V. Lotsch,  
3 *Ann. Rev. Mater. Res.* **2015**, *45*, 85.  
4  
5  
6  
7 [114] B. Seo, G. Y. Jung, Y. J. Sa, H. Y. Jeong, J. Y. Cheon, J. H. Lee, H. Y. Kim, J. C. Kim,  
8 H. S. Shin, S. K. Kwak, S. H. Joo, *ACS Nano* **2015**, *9*, 3728.  
9  
10  
11 [115] H. Liu, B. Xu, J. M. Liu, J. Yin, F. Miao, C. G. Duan, X. G. Wan, *Phys. Chem. Chem.*  
12 *Phys.* **2016**, *18*, 14222.  
13  
14  
15 [116] a) D. Ravelli, D. Dondi, M. Fagnoni, A. Albin, *Chem. Soc. Rev.* **2009**, *38*, 1999; b) J.  
16 Ran, J. Zhang, J. Yu, M. Jaroniec, S. Z. Qiao, *Chem. Soc. Rev.* **2014**, *43*, 7787.  
17  
18  
19 [117] X. Wang, K. Maeda, A. Thomas, K. Takanabe, G. Xin, J. M. Carlsson, K. Domen, M.  
20 Antonietti, *Nat. Mater.* **2009**, *8*, 76.  
21  
22  
23 [118] D. Voiry, H. Yamaguchi, J. Li, R. Silva, D. C. B. Alves, T. Fujita, M. Chen, T. Asefa,  
24 V. B. Shenoy, G. Eda, M. Chhowalla, *Nat. Mater.* **2013**, *12*, 850.  
25  
26  
27 [119] D. Voiry, M. Salehi, R. Silva, T. Fujita, M. Chen, T. Asefa, V. B. Shenoy, G. Eda, M.  
28 Chhowalla, *Nano Lett.* **2013**, *13*, 6222.  
29  
30  
31 [120] a) Y. Zheng, Y. Jiao, Y. Zhu, L. H. Li, Y. Han, Y. Chen, A. Du, M. Jaroniec, S. Z.  
32 Qiao, *Nat. Commun.* **2014**, *5*, 3783; b) Y. Jiao, Y. Zheng, M. Jaroniec, S. Z. Qiao, *Chem. Soc.*  
33 *Rev.* **2015**, *44*, 2060.  
34  
35  
36 [121] J. Duan, S. Chen, B. A. Chambers, G. G. Andersson, S. Z. Qiao, *Adv. Mater.* **2015**, *27*,  
37 4234.  
38  
39  
40 [122] L. Wang, Z. Sofer, J. Luxa, D. Sedmidubský, A. Ambrosi, M. Pumera, *Electrochem.*  
41 *Commun.* **2016**, *63*, 39.  
42  
43  
44  
45  
46  
47  
48  
49  
50  
51  
52  
53  
54  
55  
56  
57  
58  
59  
60  
61  
62  
63  
64  
65

((Insert Figure here. Note: Please do not combine figure and caption in a textbox or frame.))



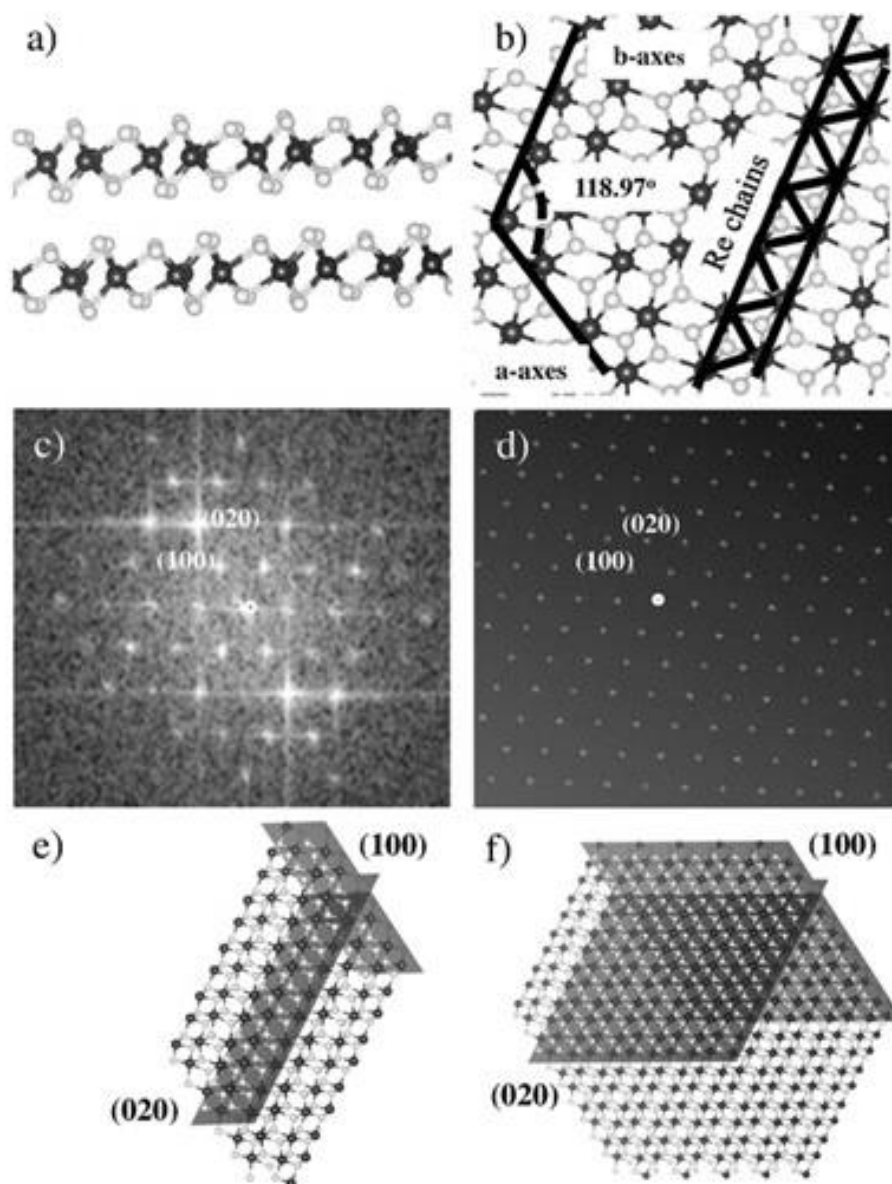
H																	He
Li	Be											B	C	N	O	F	Ne
Na	Mg											Al	Si	P	S	Cl	Ar
K	Ca	Sc	Ti	V	Cr	Mn	Fe	Co	Ni	Cu	Zn	Ga	Ge	As	Se	Br	Kr
Rb	Sr	Y	Zr	Nb	Mo	Tc	Ru	Rh	Pd	Ag	Cd	In	Sn	Sb	Te	I	Xe
Cs	Ba	Ln	Hf	Ta	W	Re	Os	Ir	Pt	Au	Hg	Tl	Pb	Bi	Po	At	Rn
Fr	Ra	An	Rf	Db	Sg	Bh	Hs	Mt	Ds	Rg							
			La	Ce	Pr	Nd	Pm	Sm	Eu	Gd	Tb	Dy	Ho	Er	Tm	Yb	Lu
			Ac	Th	Pa	U	Np	Pu	Am	Cm	Bk	Cf	Es	Fm	Md	No	Lr

**Figure 1.** Ball and stick diagram of a typical TMD. 2D Transition metals atoms (green) and chalcogen atoms (orange). Reproduced with permission from ref. 14. Copyright © 2015, Nature Publishing Group.<sup>[14]</sup>



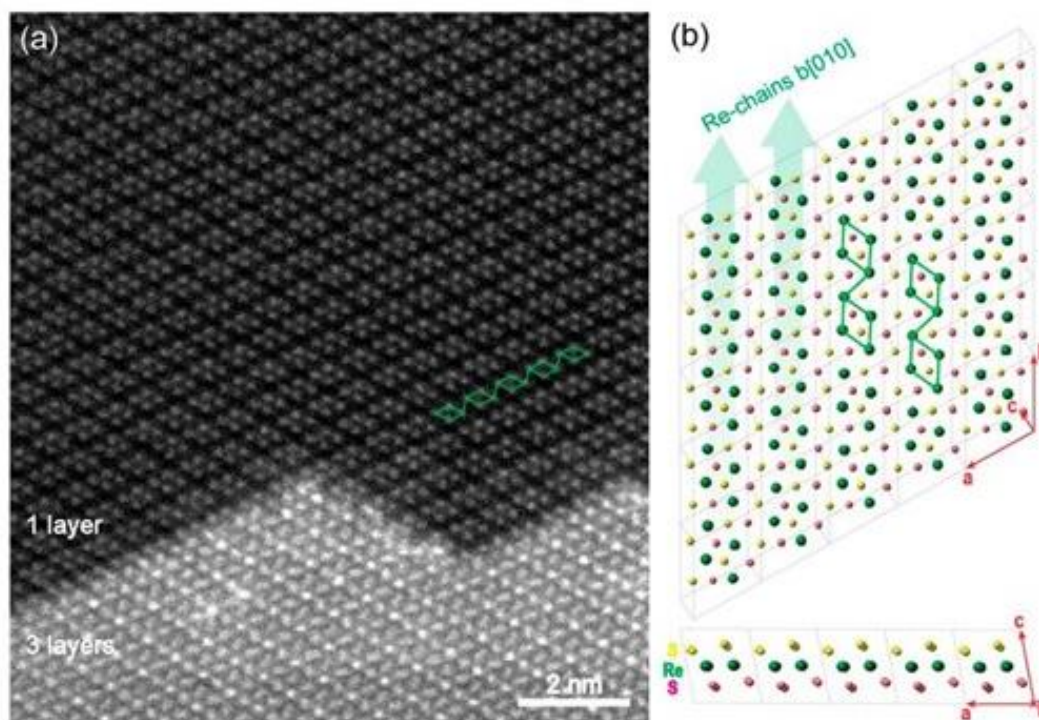
**Figure 2.** Schematic for a) Tellurium-assisted CVD growth approach and b) Surface reaction during epitaxial growth process of  $\text{ReS}_2$  atomic layer on mica. Reproduced with permission from ref. 38. Copyright © 2016, Wiley-VCH. <sup>[38]</sup>



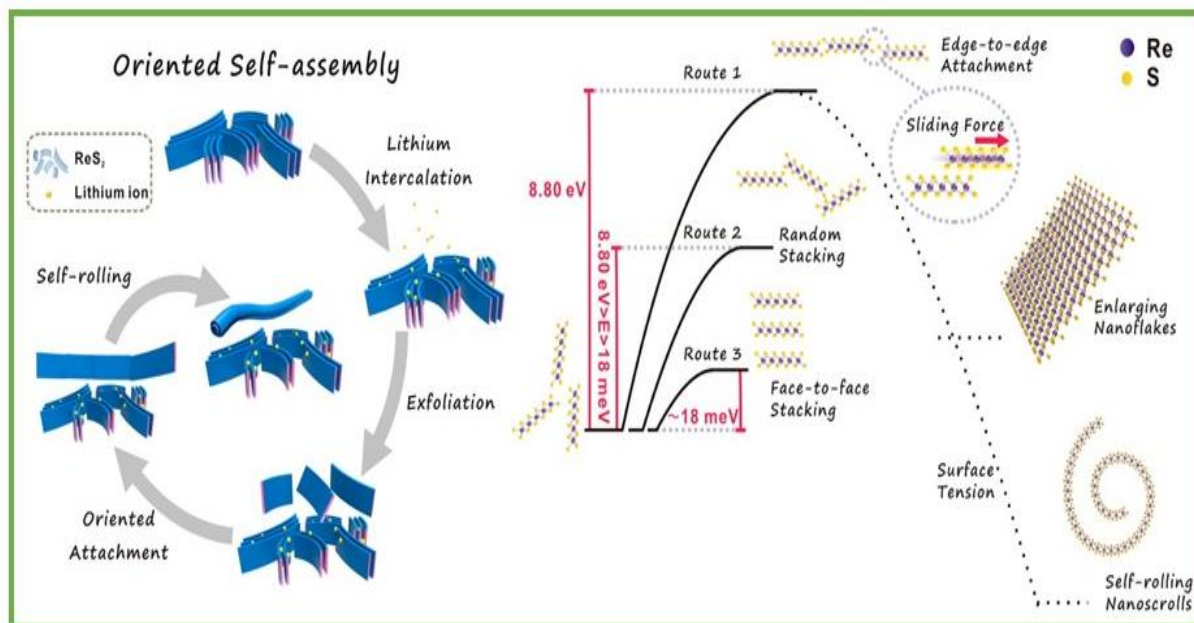


**Figure 3.** a,b) Side and top view of distorted 1 T crystal structure of  $\text{ReS}_2$ , both a and b axes and formation of Re chains as a result of Peierls distortion are denoted. Fast Fourier transform images from the c) experimental and d) simulated, structures are shown. Structural visualization was performed by using VESTA software for two different growth morphologies, e) nanorods, and f) hexagons. Reproduced with permission from ref. 42.

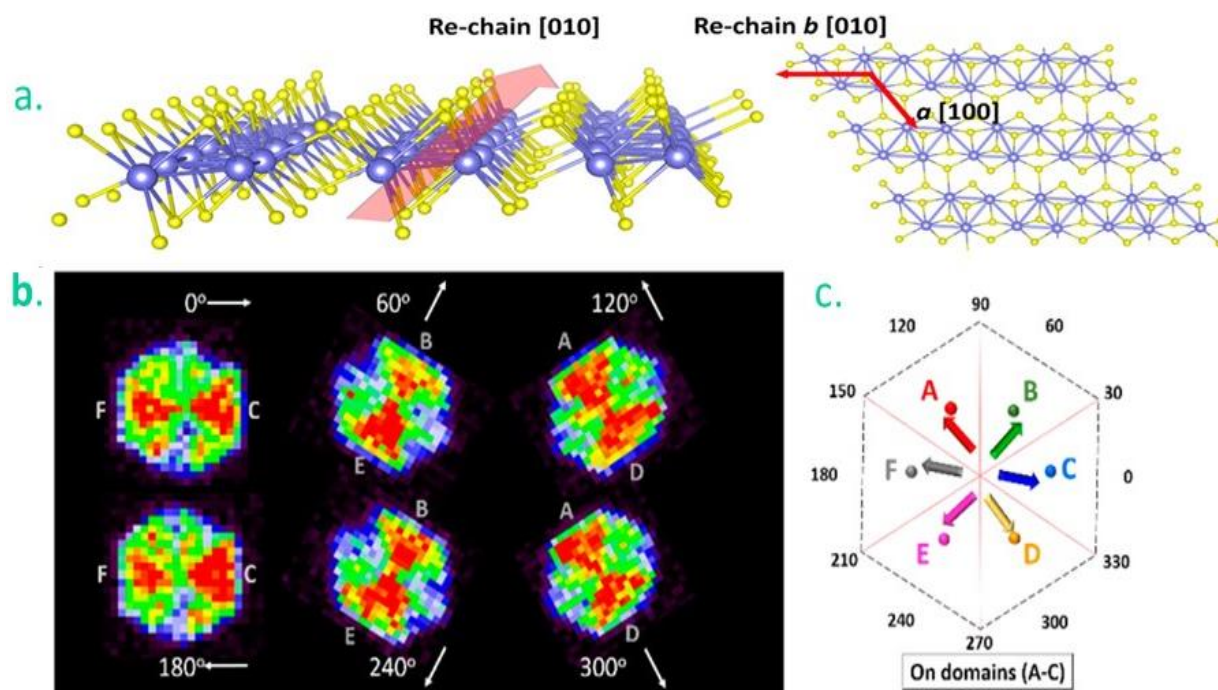
Copyright © 2016, Wiley-VCH. <sup>[42]</sup>



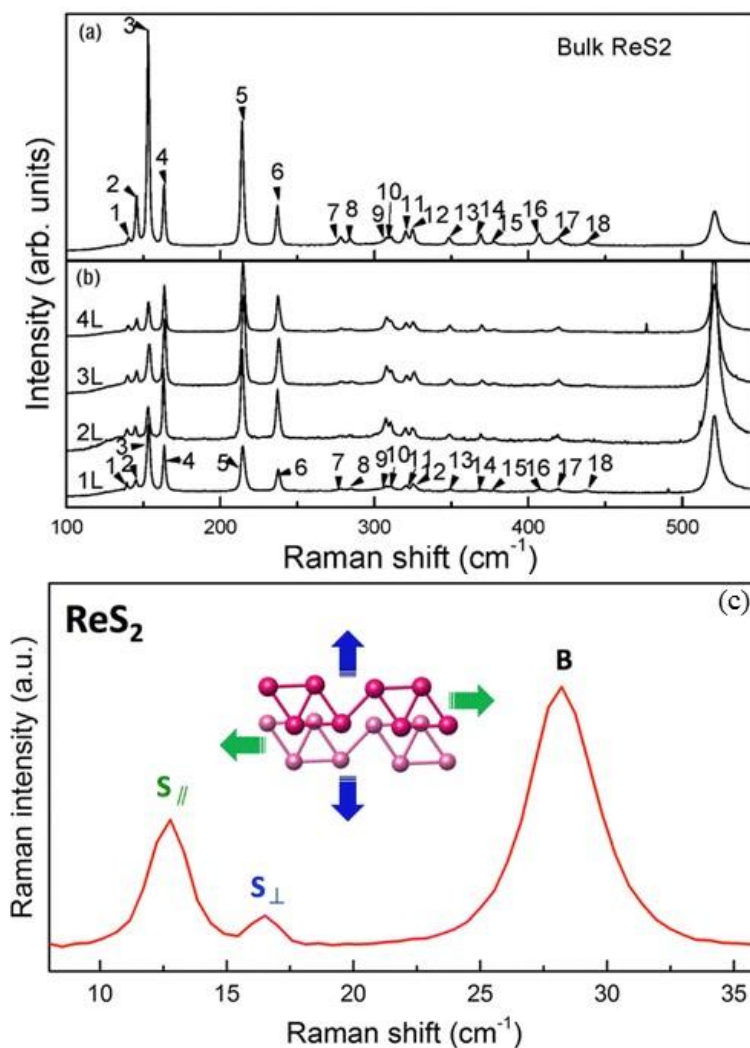
**Figure 4.** Lattice structure of ReS<sub>2</sub>. a) Transmission electron microscope image and b) schematic illustration. Reproduced with permission from ref. 13. Copyright © 2015, American Chemical Society.<sup>[13]</sup>



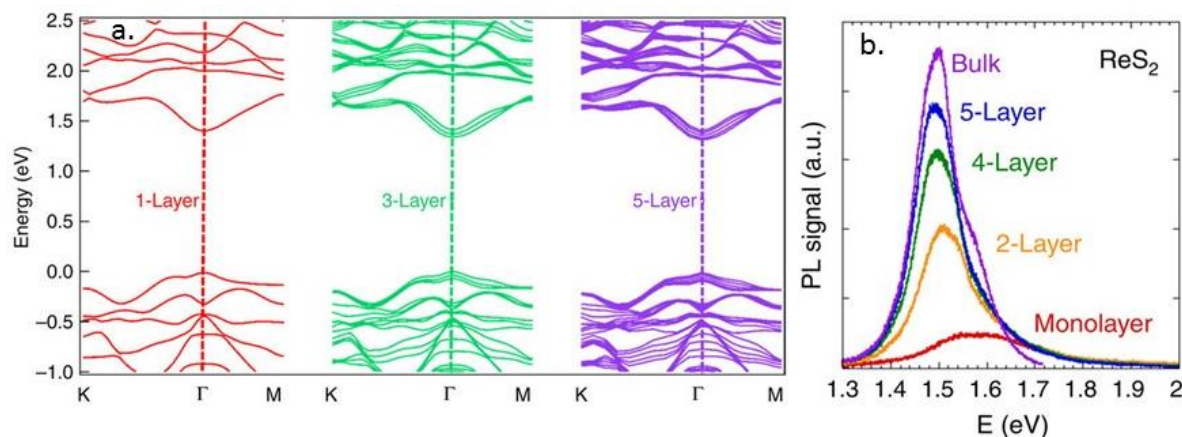
**Figure 5.** Process of edge-to-edge self-assembly orientation of  $\text{ReS}_2$  nanoscrolls. Reproduced with permission from ref. 56. Copyright © 2016, American Chemical Society. <sup>[56]</sup>



**Figure 6.** a) Schematic depiction of monolayer ReS<sub>2</sub> identifying *b*-axis [010] Re-chain direction and *a*-axis [100] across Re-chains. b) Angle-resolved nano-Raman and reflectivity spectroscopy mapping data at 214 cm<sup>-1</sup> peak at different polarization angles. Angle refers to that between the *b*-axis lattice chain direction and the polarization vector. c) Construction of grain boundaries (black dashed line) and Re-chain direction in each subdomain. Reproduced with permission from ref. 58. Copyright © 2016, American Chemical Society.<sup>[58]</sup>



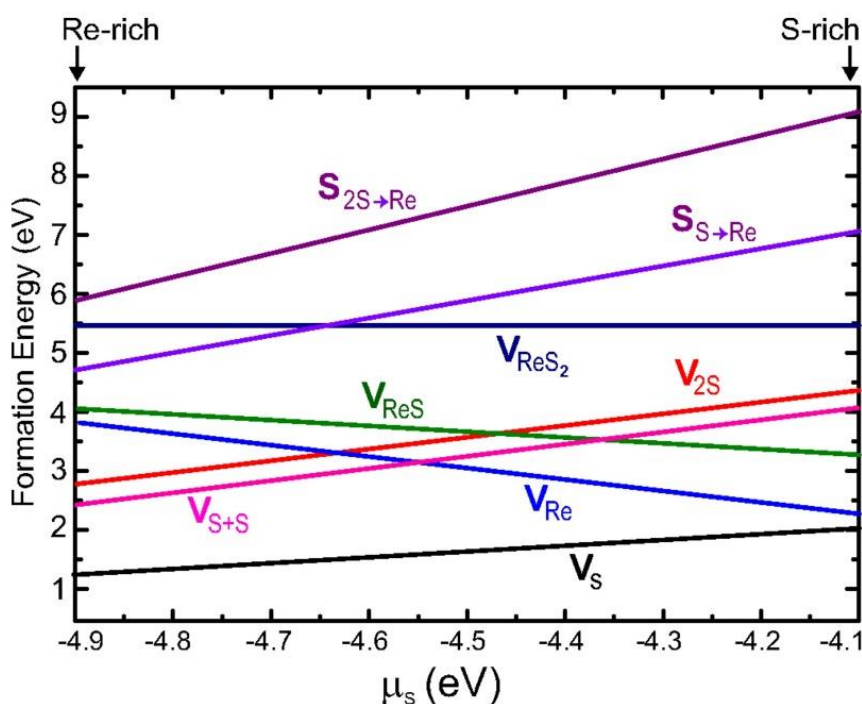
**Figure 7.** High-frequency ( $> 100 \text{ cm}^{-1}$ ) Raman spectra for (a-b) bulk and few layers ReS<sub>2</sub>, respectively, and (c) low-frequency ( $< 40 \text{ cm}^{-1}$ ) Raman spectra for 2 layers ReS<sub>2</sub>. Figure X a, b has been reproduced with permission from ref. 62. Copyright © 2015, American Physical Society. Figure Xc has been reproduced with permission from ref. 54. Copyright © 2016, American Chemical Society.<sup>[54, 62]</sup>



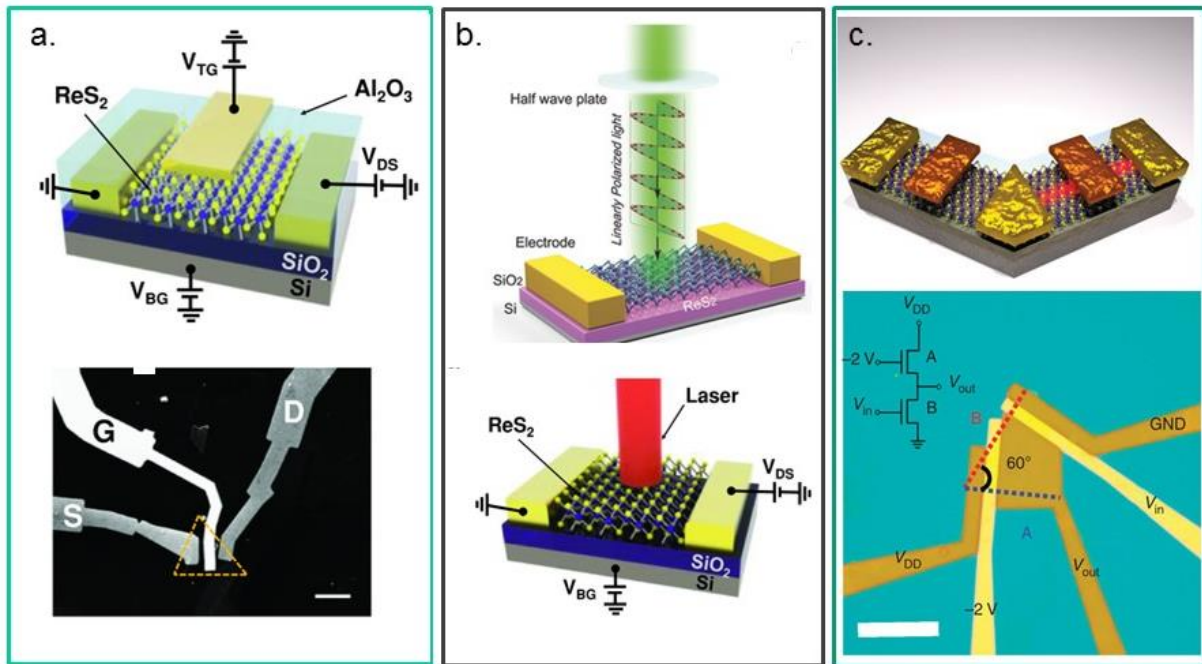
**Figure 8.** a) Band structure and b) Photoluminescence spectra of bulk and monolayer ReS<sub>2</sub>.

Figure 8a has been reproduced with permission from ref. 26 while Figure 8b from ref. 20

Copyright © 2015 and 2014, respectively, Nature Publishing Group.<sup>[20, 26]</sup>



**Figure 9.** Formation energies of vacancy (V) and substitutional (S) point defects as a function of the S chemical potential. Reproduced with permission from ref. 50. Copyright © 2014, American Physical Society.<sup>[50]</sup>



**Figure 10.** a) Schematic structure of ReS<sub>2</sub> top-gate FET (top). SEM image of the fabricated top-gate FET based on few-layer ReS<sub>2</sub> (bottom). Scale bar, 5  $\mu\text{m}$  b) 3D schematic view of the ReS<sub>2</sub> based photodetectors c) Schematic of the structure of an inverter combining two top-gated anisotropic ReS<sub>2</sub> FETs (top). Optical image of a typical inverter device, scale bar 10  $\mu\text{m}$ . Inset: the circuit diagram of the inverter (bottom). Fig. 10a Reproduced with permission from ref. 89. Copyright © 2015, Wiley-VCH. Fig. 10b Reproduced with permission from ref. 90. Copyright © 2016, Wiley-VCH. Fig. 10c Reproduced with permission from ref. 26. Copyright © 2015, Nature Publishing Group. <sup>[26, 89, 90]</sup>

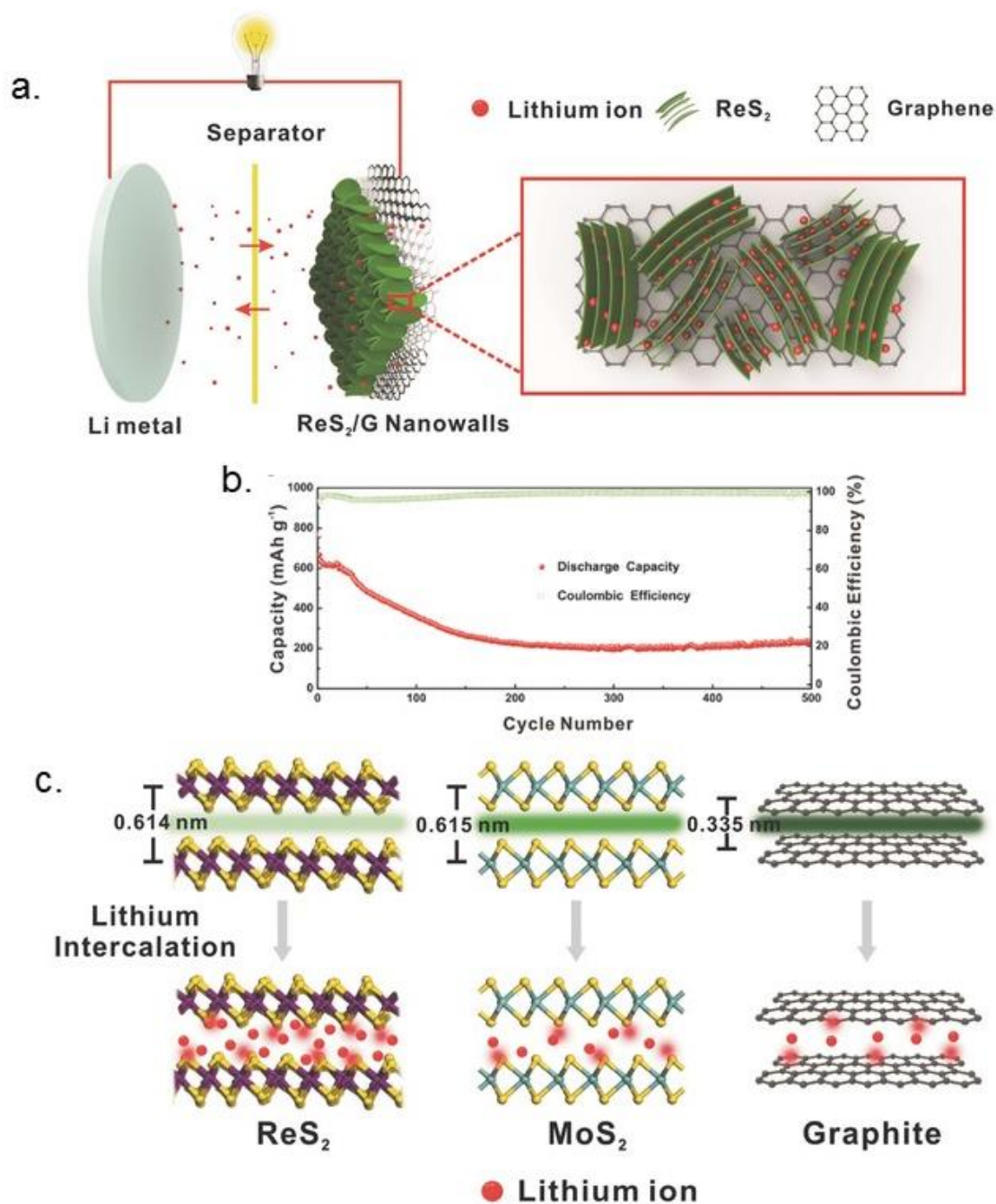


**Figure 11.** a) Schematic illustration of lithium intercalation in ReS<sub>2</sub>/3DGF-based LIB b) Long-term cycling performance of V- ReS<sub>2</sub>/3DGF composite at a current density of 1000 mA g<sup>-1</sup> c) Schematic illustration of the weak interlayer interaction of ReS<sub>2</sub>, compared with MoS<sub>2</sub> and graphite. Reproduced with permission from ref. 102. Copyright © 2016, Wiley-VCH.<sup>[102]</sup>



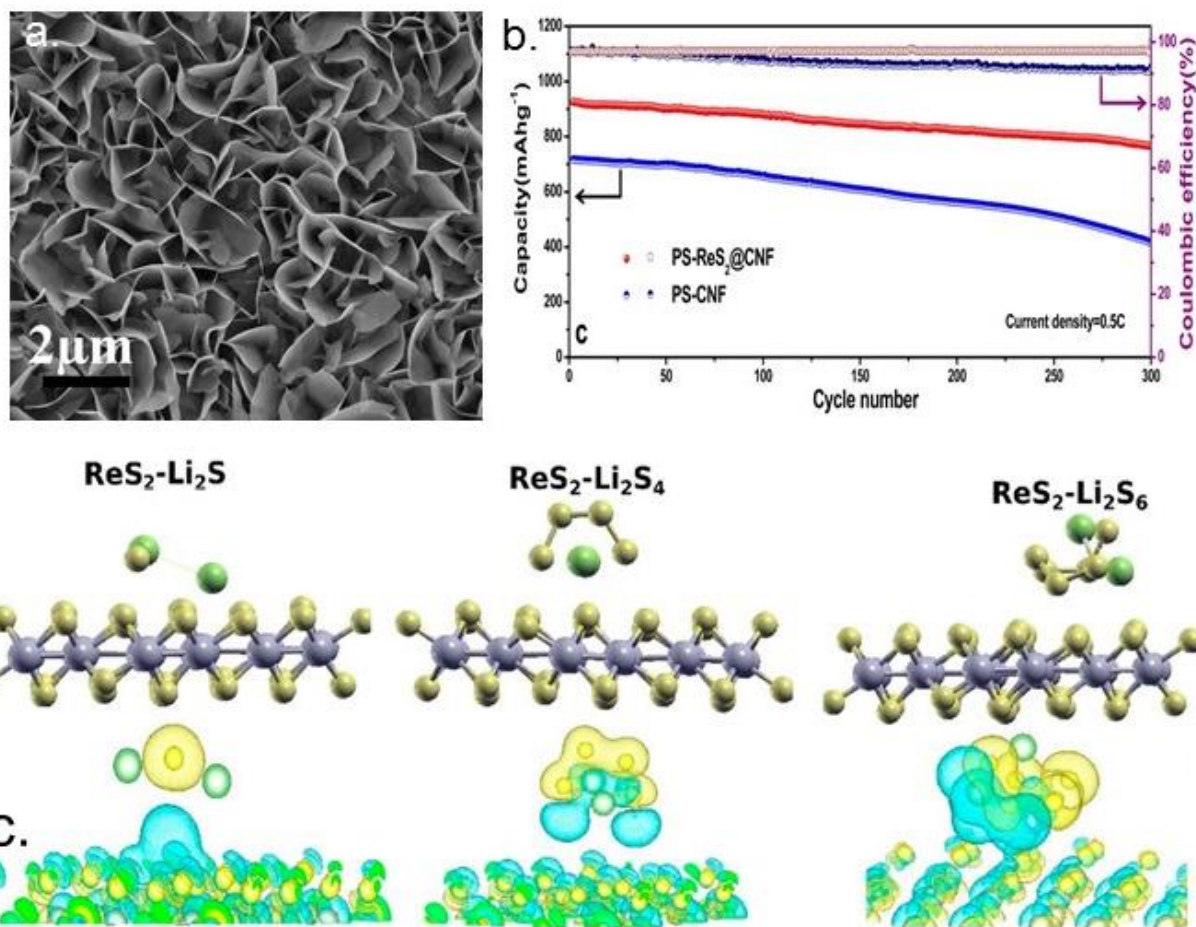


**Figure 12.** a) Vertically grown ReS<sub>2</sub> sheet for Li-S batteries b) Cycling stability and Coulombic efficiency of Li-S batteries c) Polysulfide– ReS<sub>2</sub> interactions. Reproduced with permission from ref. 107. Copyright © 2016, American Chemical Society. <sup>[107]</sup>

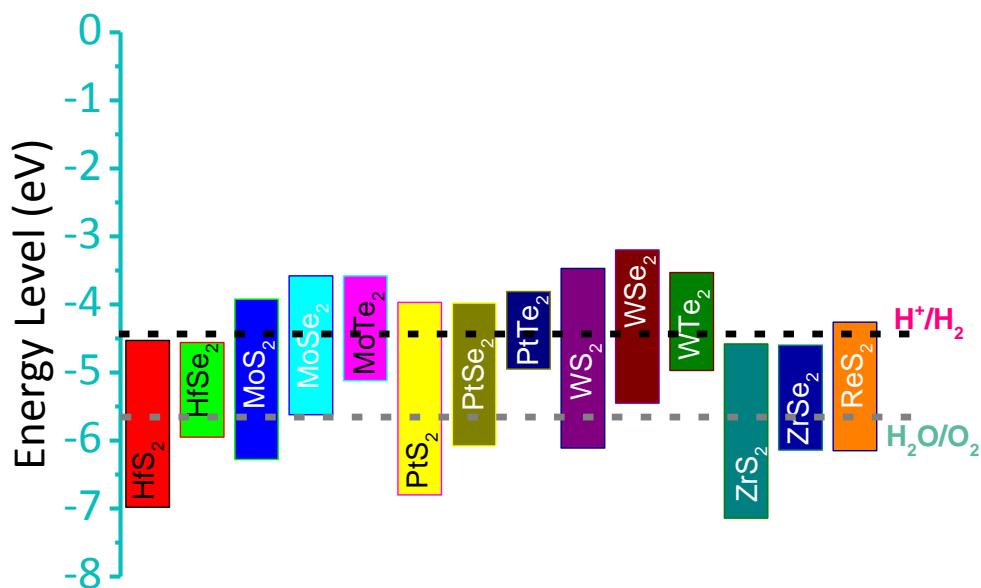


**Figure 13.** Band edges of TMDs photocatalysts. The upper end of each bar represents the CBM position while the lower end for VBM. The black-broken line corresponds to the minimum potential required for proton reduction to hydrogen molecules. The grey-broken line is for minimum oxidation potential. Based on the CBM and VBM position, three types of reactions are possible: (i) if only the CBM of given TMD lies above the black-broken line, the TMD has potential to produce hydrogen photocatalytically (i.e. MoSe<sub>2</sub>, MoTe<sub>2</sub>, PtTe<sub>2</sub>, WSe<sub>2</sub>, WTe<sub>2</sub>), (ii) if only the VBM of given TMD lies below the grey-broken line, the TMD has potential to produce oxygen photocatalytically (i.e. HfS<sub>2</sub>, HfSe<sub>2</sub>, ZrS<sub>2</sub>, ZrSe<sub>2</sub>), and (iii) if both CBM lies above the black-broken line and VBM lies below the grey-broken line, the TMD has potential for overall water-splitting (i.e. MoS<sub>2</sub>, PtS<sub>2</sub>, PtSe<sub>2</sub>, WS<sub>2</sub>, ReS<sub>2</sub>).

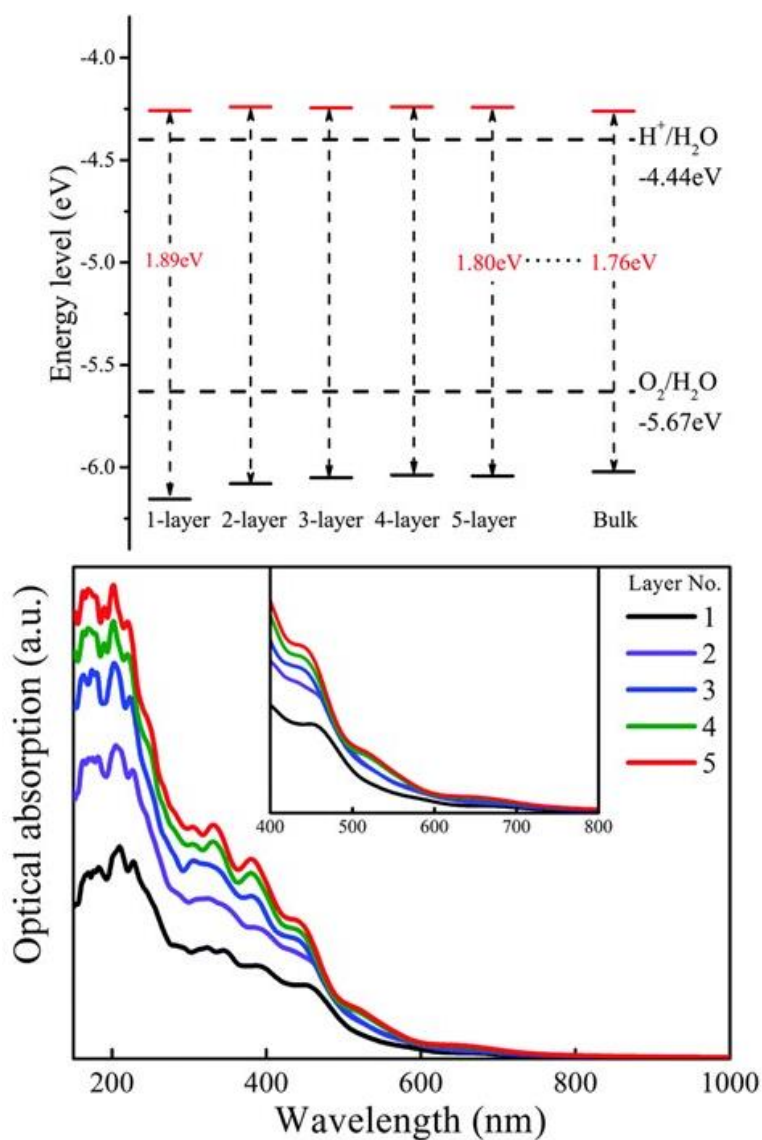


**Figure 14.** Band edge positions of multilayer  $ReS_2$  relative to the vacuum level and corresponding optical absorption. Reproduced with permission from ref. 115. Copyright © 2016, Royal Society of Chemistry. <sup>[115]</sup>

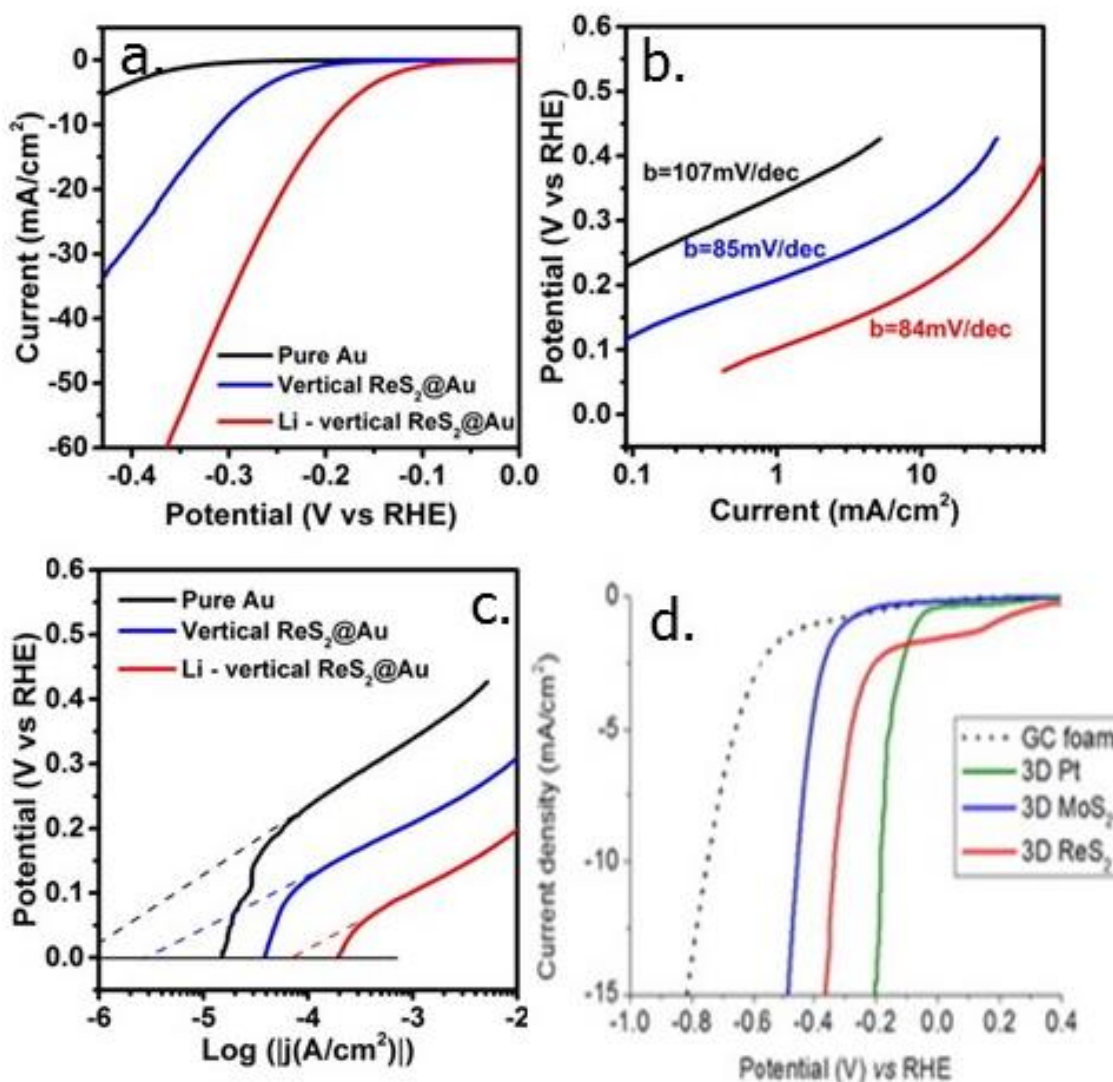


**Figure 15.** a) Polarization curves obtained with lithiated vertical ReS<sub>2</sub>@Au, as-prepared vertical ReS<sub>2</sub>@Au, and pure Au foil. b) The corresponding Tafel plots. c) Extrapolated exchange-current densities from Tafel plots d) LSV of carbon foam, 3D Pt, 3D ReS<sub>2</sub>, and 3D MoS<sub>2</sub> in N<sub>2</sub>-saturated 0.5 M H<sub>2</sub>SO<sub>4</sub>. Scan rate: 2 mV/s. Fig. 15 a-c is reproduced with permission from ref. 107. Copyright © 2016, American Chemical Society. Fig. 15 d is reproduced with permission from ref. 122. Copyright © 2016, Elsevier.<sup>[107, 122]</sup>

**Table 1.** Structural parameter of unit cell of ReS<sub>2</sub>.<sup>[24]</sup>

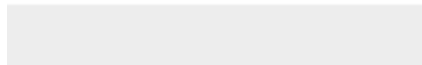
Parameter	Value
$a, \text{Å}$	6.417
$b, \text{Å}$	6.510
$c, \text{Å}$	6.461
$\alpha, \text{deg}$	121.10
$\beta, \text{deg}$	88.38
$\gamma, \text{deg}$	106.47
$V, \text{Å}^3$	219.3
$Z$	4
Space group	$P\bar{1}$
$\lambda, \text{Å}$	0.71073
$\mu, \text{mm}^{-1}$	56.84

**Table 2.** The 18 Raman active frequencies in bulk and monolayer ReS<sub>2</sub> under 633 nm solid state laser excitation.<sup>[62]</sup>

<b>Symmetry</b>	<b>Bulk Raman frequency [cm<sup>-1</sup>]</b>	<b>Monolayer Raman frequency [cm<sup>-1</sup>]</b>	<b>Origin of phonon mode</b>
<i>A<sub>g</sub></i>	140.3	139.2	Out-of-plane vibrations of Re atoms
<i>A<sub>g</sub></i>	145.9	145.3	Out-of-plane vibrations of Re atoms
<i>E<sub>g</sub></i>	153.1	153.6	In-plane vibrations of Re atoms
<i>E<sub>g</sub></i>	163.6	163.6	In-plane vibrations of Re atoms
<i>E<sub>g</sub></i>	217.2	217.7	In-plane vibrations of Re atoms
<i>E<sub>g</sub></i>	237.1	237.7	In-plane vibrations of Re atoms
<i>C<sub>p</sub></i>	278.3	278.3	In-plane and out-of-plane vibration of Re and S atoms
<i>C<sub>p</sub></i>	284.2	284.7	In-plane and out-of-plane vibration of Re and S atoms
<i>E<sub>g</sub></i>	307.8	307.8	In-plane vibrations of S atoms
<i>E<sub>g</sub></i>	311.0	311.0	In-plane vibrations of S atoms
<i>C<sub>p</sub></i>	320.6	320.6	In-plane and out-of-plane vibration of S atoms
<i>C<sub>p</sub></i>	324.9	324.9	In-plane and out-of-plane vibration of S atoms
<i>C<sub>p</sub></i>	348.8	348.8	In-plane and out-of-plane vibration of S atoms
<i>C<sub>p</sub></i>	368.9	369.5	In-plane and out-of-plane vibration of S atoms
<i>C<sub>p</sub></i>	377.9	377.4	In-plane and out-of-plane vibration of S atoms
<i>C<sub>p</sub></i>	407.3	408.3	In-plane and out-of-plane vibration of S atoms
<i>A<sub>g</sub></i>	418.7	419.3	Out-of-plane vibrations of S atoms
<i>A<sub>g</sub></i>	438.0	437.5	Out-of-plane vibrations of S atoms



Click here to access/download  
**Supporting Information**  
TOC.doc





Click here to access/download  
**Supporting Information**  
Copy rights.pdf








Click here to access/download  
**Production Data**  
Figures.docx





Click here to access/download  
**Production Data**  
authors bio.docx

